

A MONTE CARLO SIMULATION OF THE
IMPULSIVELY STARTED PISTON PROBLEM

A THESIS
IN
MECHANICAL ENGINEERING

PRESENTED TO THE FACULTY OF GRADUATE
STUDIES AND RESEARCH OF THE
UNIVERSITY OF MANITOBA
IN PARTIAL FULFILLMENT OF THE REQUIREMENTS FOR THE
DEGREE OF MASTER OF SCIENCE

BY
DOUGLAS W. RUTH

1972



SUMMARY

The computer simulation of the gas dynamic problem of an impulsively started piston in both a "hard sphere" gas and a neutral plasma is investigated by means of a new and more general Monte Carlo model. The model allows the evaluation of non-constant binary collision cross-sections. The hard sphere results take the form of a shock wave. The neutral plasma results show two discontinuities, one in each gas component. Both studies show good agreement with experimental and logical results.

The hard sphere model is then used to obtain property variations through the shock wave by means of which the Boltzmann equation is solved. The Boltzmann equation is represented in the BGK formulation with the ellipsoidal formulation for the distribution of velocities coming out of collision given by Holway. This solution proves to be a refinement over that of the Krook formulation.

ACKNOWLEDGEMENTS

I would like to express my deep appreciation to Dr. A. K. Macpherson who acted as my supervisor for this thesis. I would also like to thank Dr. R. Azad and Dr. W. M. Boerner, the members of my advisory committee, for their time and advice during both the research and writing of this work.

I would like to thank the staff and students of the Mechanical Engineering Department for their many suggestions and criticisms. Especially among them, I would like to thank Mr. G. V. Price and Mr. T. A. Derbentli.

I would like to acknowledge my gratitude to the staff of the Computer Department for their time and co-operation especially those operators who worked the weekend overtime shifts in order that the longer programs could be completed.

Finally, I would like to thank my wife, Beverly, not only for typing and proofreading the manuscript but also for helping me through the frustrations of the research.

TABLE OF CONTENTS

SUMMARY	i
ACKNOWLEDGEMENTS	ii
TABLE OF CONTENTS	iii
NOMENCLATURE	v
1. INTRODUCTION	1
PART I THE MONTE CARLO SIMULATION	8
2. THE MONTE CARLO SIMULATION MODEL	9
2.1 The General Model	9
2.2 The Computer Model for Hard Sphere Molecules	16
2.2.2 The Determination of the Time Step Parameter	17
2.3 The Neutral Plasma Simulation Model	20
2.3.1 Introduction	20
2.3.2 The Two Fluid Model For Neutral Plasma Problems	23
2.3.3 The Theoretical Resultant Behavior For an Impulsively Started Piston in a Neutral Plasma	25
2.3.4 The Time Step Parameter	26
3. SIMULATION MODEL RESULTS	29
3.1 The Hard Sphere Gas Model	29
3.1.1 The Variation of Shock Properties with Time Step Parameter	29
3.1.2 The Accuracy of the Computer Model	30
3.1.3 The Shock Structure	34
3.1.4 A Comparison of the Presented Monte Carlo Model to Other Monte Carlo Models	35
3.2 The Neutral Plasma Model	36
PART II THE BOLTZMANN EQUATION	39
4. THE BOLTZMANN EQUATION AND IT'S SOLUTION	40
5. DISCUSSION OF RESULTS	45
PART III CONCLUDING REMARKS	48
6. CONCLUDING REMARKS	49
REFERENCES	54
TABLES AND FIGURES	57

APPENDIX I	<u>Derivation of the Particles' Velocity Components After A Binary Collision</u>	86
APPENDIX II	<u>A Derivation of the One-Dimensional Statistically Modeled Boltzmann Equation</u>	89
APPENDIX III	<u>A Derivation of the One Component Velocity Distribution Function of Molecules Coming Out Of Collision</u>	92

NOMENCLATURE

Latin Alphabet

<u>a</u>	acceleration
b	impact parameter
<u>c</u>	molecular velocity
E	electric field intensity due to a cell
F	total electric field intensity acting in a cell
f	normalized velocity distribution function
g	relative speed between two particles
k	Boltzmann's constant
M	Mach number
m	molecular mass
m'	reduced mass
N	number of model molecules
n	number density
p_c	a collision parameter (page 22)
q	charge
<u>r</u>	spacial vector
Δr	spacial increment
S	time step parameter
s	molecular radius
T	temperature
T^*	sonic temperature
t	time
t_i	pre-collision flight time

Δt	time increment
\underline{u}	flow velocity
V_M	speed of the fastest moving molecule
V_m	most probable velocity upstream of the shock
V'_m	most probable velocity downstream of the shock
V_p	piston velocity
v_r	g
X	cell width

Greek Alphabet

γ	ratio of specific heats
δ	maximum slope thickness
ϵ_0	permittivity of free space
$\underline{\underline{\epsilon}}$	tensor inverse of $\underline{\underline{\lambda}}$
η	orientation of the plane of the orbits of colliding molecules
η^*	sonic point viscosity
λ	upstream mean free path
$\underline{\underline{\lambda}}$	velocity moment matrix of molecules emerging from collision (post-collisional velocity moments)
ν	collision frequency
ξ	a random number between 0 and 1
ρ	density
σ_0	collision cross-section
σ_i	total interaction cross-section
χ	deflection angle

χ_m	minimum deflection angle
ψ	normalized velocity distribution function of particles emerging from collision

1. INTRODUCTION

The impulsively started piston problem was studied in two different gases. The results take on two different forms. For a single component gas in which the molecules are assumed to act as hard spheres, the resulting structure of the gas was that of a shock wave. For a gas composed of equal quantities of electrons and protons, the resulting structure of the gas was that of two discontinuities one in each component. The impulsively started piston problem in a hard sphere gas will henceforth be referred to as the internal structure of a shock wave problem.

The study of the internal structure of a shock wave is a scientific problem which presents many difficulties. Under standard conditions a shock in air has small dimensions ($\sim 10^{-3}$ cm thick) and moves at a high speed ($> 3 \times 10^5$ cm/sec). For these reasons, the standard procedures of measurement used by experimentalists have proved to be of little use.

Two representative studies of the experimental results concerning internal shock structure of high velocity shocks to date are those by Camac¹ and Robben and Talbot.² Both investigators studied shock density profiles and shock density thicknesses using electron beam techniques. Camac¹ performed his work in argon at Mach numbers between 5 and 10. He reported reciprocal shock wave thicknesses non-dimensionalized with upstream mean free path of between 0.181 and 0.245. He compared these results with several numerically obtained results. However, no attempt was made to present any accurate density profiles. Robben and Talbot² performed their work in helium, argon, and nitrogen over the range Mach 1.5 to 17.4. They reported reciprocal shock thicknesses non-dimensionalized with a Reynolds number based on shock thickness of 0.141 to 0.17.

They compared these results with earlier work including that of Camac.¹ Once again no attempt was made to present accurate density profiles. Both studies report that several corrections were necessary to reduce the data to a workable form.

No experimental work has been reported to date on any shock parameter except density. The only other exact information concerning shock structure are the jump conditions across the shock. These are based on continuum theory and may be found in any standard reference on compressible fluid flow, (e.g. Shapiro³).

Investigations of shock structure by means of Monte Carlo simulation models have been performed by Bird^{4,5,6} and Macpherson.^{7,8} The basis of the technique was the assumption that the behavior of a large number of molecules could be studied by studying the behavior of a small subgroup of the molecules. A system of cells was set up in which molecules were assumed to be isolated during a short time interval. During this time interval the model molecules were allowed to interact with each other within the same cell. Both investigators assumed that the time interval required for a collision to occur was

$$2/N n \sigma_0 v_r$$

where N was the number of model molecules, n was the number density, σ_0 was the collision cross-section and v_r was the relative velocity of the two colliding molecules. Both investigators assumed that the molecules acted as hard spheres and that the probability of collision was proportional to the above time interval. A much fuller account of Monte Carlo models will be given in Section 2.1.

Bird^{4,5} presented density, temperature, and velocity profiles for shocks of Mach 1.5, 3.0, and 10.0. Macpherson⁷ presented density, temperature, pressure and velocity profiles for a Mach 10.0 shock wave.

The study of magnetohydrodynamic flows is very complex. Although the basic laws of charged particle interactions, electromagnetic field behavior, radiation and other associated fields are well understood, the interactions of large numbers of charged particles is complicated. Theoretical works contain many simplifying assumptions and experimental work is hampered by high equipment costs.

Generally, magnetohydrodynamic discontinuities are treated in a macroscopic manner. Standard references such as Sutton and Sherman⁹ and Holt and Haskell¹⁰ use this approach.

The Boltzmann equation is generally written as

$$\frac{\partial f}{\partial t} + \underline{c} \cdot \frac{\partial f}{\partial \underline{r}} + \underline{a} \cdot \frac{\partial f}{\partial \underline{c}} = \left(\frac{\partial f}{\partial t} \right)_{col} \quad 1-1$$

where f is the velocity distribution function, t is the time, \underline{c} is the molecular velocity, \underline{r} is the spacial position vector, \underline{a} is the acceleration due to external forces, and the right hand side of the equation is the collision term.

One of the earliest solution attempts of the Boltzmann equation was that proposed by Enskog and independently by Chapman. The Enskog-Chapman method was described in detail in reference 11. This method expressed the distribution of molecules emerging from a collision in terms of a vector \underline{A} and a tensor $\underline{\underline{B}}$. These two quantities were then expanded

using the Sonine polynomials¹¹ which have the form

$$\sum_{i=0}^j (-x)^i (h+j)_{j-i} / i! (j-i)!$$

where j is the order of the desired polynomial, x is the independent variable and h is a number which depends on the molecular model. The solution of these series when combined in the total solution, became progressively more difficult as the order, j , increased. In effect, above order three the series was unsolvable.

Although many solutions have been presented using the Enskog-Chapman formulation, Mott-Smith¹² showed that based on work using a third order polynomial the series converged so slowly for Mach numbers larger than 1.2 that the method was not valid above this value.

Mott-Smith¹² went on to propose an alternate model. He assumed that the distribution function could be represented as a bi-modal maxwellian of the form

$$n_a f_a + n_b f_b$$

where f_a and f_b were maxwellians about different temperatures and n_a and n_b were the number density of molecules representing these maxwellians. The solution for the distribution function was performed by a first step iteration method. From these he obtained density thicknesses. He stated that his model worked best for Mach numbers higher than 2.0.

The collision term of the Boltzmann equation was modeled by Bhatnagar, Gross, and Krook¹³ as

$$v(\psi - f)$$

where v was the collision frequency and ψ was the velocity distribution

of molecules emerging from collision. This is the well known BGK approximation. Furthermore, Krook¹⁴ proposed that ψ at any position be approximated by the maxwellian distribution corresponding to the temperature at that position. He suggested that steady state problems could then be solved by determining v and T , the temperature, in the same manner as they were determined for solving the Enskog-Chapman model (see reference 11).

Anderson¹⁵ used the BGK formulation of Boltzmann's equation in a discrete analog system which he solved by an iteration procedure. His method was numerical and complicated. He did not present distribution functions, however, density, temperature, and velocity profiles were presented for Mach 1.2 and 10.0 shocks.

Holway¹⁶ used the BGK formulation, however, he derived an alternate representation for ψ . Using statistical arguments he showed that ψ could be represented as a function of the velocity moments of particles emerging from collision. The equation had the form

$$(2\pi)^{-3/2} |\underline{\lambda}|^{-1/2} \exp - \frac{1}{2} (\epsilon_{ij} (c_i - u_i) (c_j - u_j))$$

where $\underline{\lambda}$ was the velocity moment matrix ($v_1 v_1, v_2 v_2, v_1 v_2$, etc.) of molecules emerging from collision (often called post-collisional velocity moments), $\underline{\epsilon}$ was the tensor inverse of $\underline{\lambda}$, and \underline{u} was the flow. This formulation is often referred to as the ellipsoidal model. To solve his equation Holway¹⁶ had to resort to Enskog-Chapman techniques.

Enskog-Chapman solutions require knowledge of temperatures and collision frequencies through the shock. Since v and T are not known experimentally, all of the models except those of Mott-Smith¹² and

Anderson¹⁵ must be solved by further assumptions or by iteration techniques. The Mott-Smith¹² model defines a priori the form of f and is, therefore, limited to one type of solution. The Anderson¹⁵ solution is almost purely numerical and takes little account of physical behavior. None of the papers discussed presented actual distribution functions.

Bird⁵ used the Monte Carlo simulation technique to give the velocity distributions directly. His method required that particles be counted in both position and velocity space. Since the Monte Carlo model ran efficiently only when the number of model molecules was small, the accuracy of such an analysis was in some doubt.

The present work covered three studies. Firstly, a new and more general Monte Carlo simulation model based on a paper by Denisik et al¹⁷ was developed and analyzed. This model allowed for the definition of variable collision cross-sections.

Secondly, the general Monte Carlo model was extended to show that it was applicable to the study of phenomena in a non-equilibrium neutral plasma. The specific problem considered was that of an infinite piston impulsively entering a neutral plasma. Since this was the first model of its type, the state of the gas modeled was chosen in a simple region. Sutton and Sherman⁹ give the various plasma regimes. The gas modeled lies in the S region. In this region ionization is greater than 50%. All internal magnetic fields are ignored since their effect is very small. In this regime bremsstrahlung radiation is unimportant and no electrons have relativistic velocities. With these properties very few assumptions were needed to achieve a working model.

Thirdly, a complete solution to the Boltzmann equation was obtained

by using Monte Carlo derived shock profiles in the Krook¹⁴ formulation with the Holway¹⁶ ψ representation.

The thesis is organized into three parts. Part I describes the method and results of the two Monte Carlo models. Part II describes the Boltzmann equation solutions. All concluding remarks are presented in Part III.

PART I

THE MONTE CARLO SIMULATION

2. THE MONTE CARLO SIMULATION MODEL

2.1 The General Model

The increasing availability of high speed electronic computers has made the direct simulation of some natural phenomena feasible. The Monte Carlo technique is a statistical simulation method that assumes that a large number of molecules have the same average behavior as a small subgroup of themselves. The study of gas dynamic problems by use of this method involves modeling the behavior of such a subgroup.

A shock wave was modeled by assuming a positional space between two walls (see Figure 1). The right wall was assumed to be movable and was referred to as the piston. A cartesian co-ordinate system was originated in the left wall. Both walls were assumed to be infinite and to be perpendicular to the x axis.

Molecules were positioned in the x direction between the two walls in a totally random manner. A standard subroutine that generated rectangularly distributed random numbers between 0 and 1 was used to give fractional distances. The fractional distances were then multiplied by the total distance between the two walls to find the x component of the molecules position. It was not necessary to determine y and z positions because the shock wave was considered to be one dimensional (i.e. the shock was assumed to be infinite in the y and z directions).

The velocity space of the molecules was assigned by means of an algorithm given by Bird¹⁸ and described as follows. The velocity space was assumed to be maxwellian, therefore the probability of a molecule having a molecular speed, c , (normalized with the most probable speed)

was proportional to

$$c^2 \exp(-c^2)$$

The most probable speed therefore had a probability of occurrence of

$$\exp(-1)$$

and the ratio of probability of the occurrence of any speed to the maximum probability was

$$R = c^2 \exp(1 - c^2) \quad 2-1$$

A counter, K , was set to some initial random number between 0 and 1.

A value of c was then randomly generated, and its probability ratio,

R , was calculated. The counter was then set to

$$K = K + R \quad 2-2$$

Values of c were chosen until K was larger than 1. The final value of c was then the required value. The value of K was then adjusted to

$$K = K - 1 \quad 2-3$$

and the next molecular speed was chosen in an identical manner. The result was a Maxwellian speed distribution.

The velocity components were assigned by choosing random directional cosines and multiplying them by the molecular speeds found above.

Although the molecular speeds are generally considered, for mathematical convenience, to range from 0 to ∞ , for the purpose of the model only speeds between 0 and 6 times the most probable velocity were assumed to occur. This in fact considered over 99.99% of all molecules.

The space between the walls was assumed to be divided into a number of equal width cells. The value of any physical property, such as temperature or density, at the center position of each cell was assumed to be

represented by the average of the property over the molecules whose x positions were between the two cell boundaries.

All tests of the model were conducted using 4000 model molecules distributed over 40 cells.

The original width of each cell was determined in the following manner. The thickness of a shock wave is of approximately the same size as the mean free path in the undisturbed gas. Therefore, to obtain a reasonable approximation of the variation of properties through the shock, the cell width had to be of such a size that the shock thickness included several cell widths. However, if the cell width was too small very few collisions would occur since the mean free path would be large compared to the cell width. Based on experimentation with the model, an initial cell width of 0.7 undisturbed mean free paths was chosen. As the model is run, the cell width decreases. The above initial size was such that in a reasonable amount of computer time the model advanced to the point where the cell width was approximately 0.35 mean free paths which gave good resolution of properties. However, this initial cell spacing insured that sufficient model time elapsed so that several cells near the piston end of the system developed to post-shock maxwellian conditions.

The shock wave was generated by allowing the piston to instantaneously take a velocity of

$$V_p = \sqrt{2\gamma} \frac{(1 - M^2)}{(\gamma + 1)M} \quad 2-4$$

where γ was the specific heat ratio and M was the upstream Mach number (Bird⁴, Macpherson⁷). A piston moving at this speed created a discontinuity which had the properties of a plane normal shock in a Mach number,

M, flow. Collisions between molecules and the wall or molecules and the piston were assumed to be specular.

The value of the piston velocity was simply the difference in the flow velocity across a Mach number, M , shock wave.* For simplicity, the region on the piston side of the shock was referred to as downstream while the region on the wall side of the shock was referred to as either the upstream or the undisturbed region.

The mathematical model, used to simulate the collisions between molecules, was the basis of the simulation study. Three separate problems were associated with the molecular collisions. Firstly, the elapsed time before a collision occurred had to be calculated. Secondly, the two colliding molecules had to be identified. Thirdly, the actual interaction

* The ratio of flow velocity across a shock is

$$\frac{2 + (\gamma - 1) M^2}{(\gamma + 1) M^2}$$

The upstream flow velocity is the product of the upstream Mach number and the speed of sound which has a value of $\gamma/2 V_m$. The piston velocity which is given by the difference between the upstream flow velocity and the downstream flow velocity is then

$$M \frac{\gamma}{2} V_m \left(\frac{2 + (\gamma - 1) M^2}{(\gamma + 1) M^2} - 1 \right)$$

which when divided by V_m , the most probable upstream velocity, and simplified yields

$$\frac{2 \gamma (1 - M^2)}{(\gamma + 1) M}$$

of the two molecules or in actuality the final velocity components after interaction had to be defined.

Denisik et al¹⁷ proposed that the time of flight before collision for any molecule could be expressed as

$$t_i = \frac{N \ln \xi_i}{n \sigma_i c_i} \quad 2-5$$

where ξ_i was a random number between 0 and 1, N was the number of model molecules in the cell, n was the cell's number density, c_i was the speed of the molecule considered, and σ_i was the total interaction cross-section of the molecule given by

$$\sigma_i = \sum_{j=1}^N \left| \frac{c_i - c_j}{c_i} \right| \sigma_{0ij} \quad 2-6$$

where σ_{0ij} was the interaction cross-section between the i -th and j -th molecules. This differs in several ways from the time of flight used in previous models.

Both Bird⁴ and Macpherson⁷ used a time interval of

$$t_i = 2/(N n \sigma_0 v_r) \quad 2-7$$

The new formulation, (equation 2-5), had several advantages over the earlier formulation, (equation 2-7). Firstly, the new formulation inherently considered the possibility of the collision of a particle with every other particle in a cell. The earlier model was based on a particle colliding with some average particle. Secondly, the new model was applicable to interaction models for which the cross-section was not constant for all collisions. This was possible in the old formulation only by using an average evaluation of σ_0 . Thirdly, the new formulation

inherently considered the random nature of collisions, whereas, the former model did not. The new formulation was, therefore, both more exact and more flexible.

The primary collision partner was found by first evaluating equation 2-5 for all molecules in a cell. The molecule, for which t_i was a minimum, was then the primary collision partner. The secondary collision partner was chosen at random with a probability proportional to

$$\frac{|c_i - c_j| \sigma_{0ij}}{2 V_M \sigma_M}$$

where V_M was the speed of the fastest moving molecule in the cell and σ_M was the maximum interaction cross-section in the cell.

Appendix I contains a derivation of the components of velocity after collision. Therein, it is shown that the collision is completely defined by the deflection angle, χ , and the orientation of the plane of the orbits of the colliding molecules, η . Since both hard spheres and coulomb particles have symmetric force fields, η was chosen at random between 0 and 2π . The manner in which the deflection angle was chosen depended on the assumed interparticle force law.

Once the initial system was set up, the computer simulation model proceeded as follows. For a certain time increment, Δt , each cell was assumed to be an isolated system. During this time only particles within any one cell could interact with each other. Molecular movement was not considered during this increment. Collisions were simulated in each cell until the sum of the collision times, t_i , given by equation 2-5 was larger than the time increment. After each cell had been considered,

the position of the piston resulting from movement at the velocity given by equation 2-4 for Δt was calculated. The new positions of the molecules were then calculated using the equation

$$x = x_0 + v \Delta t + \frac{a \Delta t^2}{2} \quad 2-8$$

where 0 denoted conditions at the beginning of the time increment and a was the acceleration of the particle due to external force fields. At this stage, collisions with the wall and the piston were considered. These collisions were calculated in detail as to when during the time increment they occurred. If an acceleration was present, all velocities were increased to

$$v = v_0 + a \Delta t \quad 2-9$$

After all the molecules were relocated, the cell boundaries were redefined and each molecule was identified as to which cell it was located in. All physical parameters of interest were then calculated. These steps were repeated until the required data was acquired.

No analytic arguments have been presented that satisfactorily define the magnitude of the time increment, Δt . Bird⁵ suggested it should be small relative to the mean collision free time. Macpherson⁷ suggested that the fastest molecule be allowed to move 0.4 - 0.5 of a cell width. This value was later raised to 0.7. The ultimate determination of Δt had to be made through experimental testing of the model. However, several logical arguments were presented to determine limits to the magnitude of Δt . These arguments are found in Section 2.2.2.

If the time increment was too long the molecules in each cell would actually move far outside of the cell boundaries during the time step.

This would violate the isolation assumption. If the time increment was too short insufficient collisions would occur. The result would be that particles acquiring energy from the piston would penetrate far upstream before transferring energy to other particles. This would cause the shock to be poorly defined as to shape and size. Also downstream Maxwellian conditions would not result since little or no energy would be transferred into the y and z directions.

The time increment was defined as

$$\Delta t = \frac{S X}{V_M} \quad 2-10$$

where S was a constant, henceforth referred to as the time step parameter, X was the cell width, and V_M was the speed of the fastest moving particle in the system. The limits of S were found by logical arguments and the final value of S was found by experimentation with the model.

2.2 The Computer Model For Hard Sphere Molecules

2.2.1 Introduction

The study of gas dynamics by assuming that molecules act as rigid hard spheres dates back several centuries. The hard sphere gas approximation allows the evaluation of almost all properties of a gas in a steady state. By incorporating these properties in a Monte Carlo scheme, information about non-steady conditions may be obtained.

Assuming the molecular sphere had a radius of s, the interaction cross-section in equation 2-6 was given by

$$\sigma_{Oij} = 4\pi s^2 \quad 2-11$$

which was a constant for all interactions. The impact parameter varied between 0 and $2s$ with a probability of occurrence proportional to itself (i.e. the probability of a collision impact parameter of b is proportional to $b \pi db$. Since πdb is a constant, the probability of occurrence of b is proportional to itself). Once b was chosen, the deflection angle, χ , followed immediately since

$$\chi = \pi - 2 \sin^{-1} \left(\frac{b}{2s} \right) \quad 2-11$$

This completed the defining of the Monte Carlo model as described in Section 2.1.

It was immediately evident that the deflection angle, χ , was not dependent on the magnitude of s , but only on the fact that $b/2s$ varied from 0 to 1. The only physical property of interest which depended on σ_{0ij} was the collision frequency. By assuming $s = 1 \times 10^{-8}$ the collision frequency was in effect non-dimensionalized with a one angstrom molecular radius. The Monte Carlo model of hard sphere molecules was therefore independent of the molecular radius assumed.

The hard sphere gas model was tested extensively to determine its applicability to the study of shock waves. All tests were conducted for a Mach number 10 shock in a gas with a number density of 10^{18} molecules per cubic centimeter.

2.2.2 The Determination of the Time Step Parameter

For a hard sphere gas, logical arguments will be presented to determine approximate upper and lower limits for S .

The collision frequency in any cell was found by counting the number

of model collisions occurring in the cell and multiplying by

$$\frac{2}{N \Delta t}$$

where N was the number of model molecules in the cell and Δt was the time increment. If no model collisions occurred, the predicted collision frequency would be zero which is an inaccurate prediction caused by the fact that the model is discrete (i.e. assuming one model molecule represents one hundred real molecules, one model collision represents one hundred collisions. However, fifty real collisions could not be modeled since the model molecule cannot experience half of a collision). The minimum collision frequency occurred upstream of the shock and had a magnitude of 2005 collisions per particle per second non-dimensionalized with the most probable upstream molecular velocity.* It was felt unreasonable to allow less than one collision per four cells in this region. An average over four data sets then resulted in an average of one collision per cell.

When the cell width was approximately 0.35 of the initial mean free path, the number of particles in each upstream cell was approximately 50. The upstream mean free path was 0.56×10^{-3} cm for a number density of 10^{18} particles per cc. From equation 2-10 and the collision frequency

* This follows from the hard sphere collision frequency

$$4 n s^2 (\pi k T/m)^{1/2}$$

by considering an s of one angstrom and dividing by the most probable velocity $(2k T/m)^{1/2}$.

it follows that

$$S = \frac{2 V_M}{X \nu N} \quad 2-12$$

V_M was approximately 20 times the most probable velocity and therefore the minimum limit of S from equation 2-12 was approximately 0.5.

An upper limit for S was not as easily specified. In order to justify the isolation of each cell during a time step, it seemed logical that the maximum speed particle not be allowed to move more than one cell width. However, this stipulation may be argued to be too small since a single unusually fast particle could retard the development of the shock. On the other hand, arguing strictly on isolation terms, $S = 1.0$ is very large since a high speed particle moving to the left, located initially on the left hand boundary of the cell would move almost across the next cell. The isolation argument and the retardation argument had to be compromised.

For a maxwellian distribution 99% of the particles had speeds between 0 and $2 V_m$. The maximum speed allowed in the initial system was $6 V_m$. It was therefore possible to allow the fastest particle to cross 3 cells and still have 99% of the particles cross 1 or less cells. However, the piston imparted energy to some particles and the result was that the maximum speed in the system was approximately $20 V_m$. At the same time the downstream particles took on a maxwellian distribution whose most probable velocity, V'_m , was $5.66 V_m$. The maximum velocity particle was therefore approximately $3.5 V'_m$. Allowing the maximum speed particle to cross 3 cells in a time increment still guaranteed that over 90% of the upstream particles crossed less than one cell. It was felt therefore, that a time step of three was a logical upper limit.

The ultimate choice of the time step parameter was made by experimenting with the model. The parameter was checked at values of 0.5, 1.0, 1.5, 3.0 and 10.0. The last value was tested to determine the model's behavior far outside the logical upper limit.

2.3 The Neutral Plasma Simulation Model

2.3.1 Introduction

The investigation of non-equilibrium behavior in a neutral electron-proton plasma presented many complications that did not exist in a gas composed of uncharged particles. Many of these difficulties arose from the fact that a charged particle influences all other charged particles irregardless of how far apart these particles are.

The interactions of charged particles were considered to be of two types, close encounters or collisions and distant encounters or far field effects.

For the Monte Carlo model two collision definitions were considered. The first defined as a collision, an encounter between two particles for which the impact parameter was less than or equal to the local Debye shielding length (Sutton and Sherman⁹) given by

$$b_{\max} = \left(\frac{2 k \epsilon_0 T}{n e^2} \right)^{1/2} \quad 2-13$$

where k was the Boltzmann constant, ϵ_0 was the permitivity of free space, T was the temperature, n was the number density and e was the electron charge. The second defined a collision as an encounter between two particles for which the impact parameter was less than or equal to the radius of the sphere that enclosed the volume unique to

each particle. The volume unique to each particle was the inverse of the number density, therefore,

$$b_{\max} = \left(\frac{1}{4.189 n} \right)^{1/3} \quad 2-14$$

In any particular case the minimum of these two definitions was used.

The Debye shielding length limit was used to account for the fact that due to screening of charged particles by oppositely charged particles the effective collision cross-section was reduced. The argument for its choice is given in Sutton and Sherman.⁹ It is the same argument that leads to the screened coulomb potential definition of classical electrostatic theory.*

The unique volume definition was based on the argument that interactions between more than two particles at once could be treated as far field effects. The probability of two particles being closer to each other than to any other particles was greater than 50% only if one particle entered the other particle's unique space. Any encounters with an impact parameter larger than the radius of the unique space were not considered to be collisions.

Having defined a collision, the collision cross-section for charged particles was evaluated. It was assumed that the coulomb potential law applied for $b < b_{\max}$ and that the potential was zero for $b > b_{\max}$. This was the same approach followed by Sutton and Sherman.⁹ The

* The argument is based on the distance a charged particle's field extends before oppositely charged particles effectively shield it.

integrated form of equation 4.66* of Holt and Haskell¹⁰ then gave the collision cross-section as

$$\sigma_{0ij} = \frac{\pi}{2} p_c^2 \left(\frac{1 + \cos \chi_m}{1 - \cos \chi_m} \right) \quad 2-15$$

where

$$p_c = \frac{q_i q_j}{4\pi \epsilon_0 m' g^2} \quad 2-16$$

where q was the charge, g was the relative velocity and m' was the reduced mass

$$m' = \frac{m_i m_j}{m_i + m_j} \quad 2-17$$

χ_m denoted the minimum deflection angle and was given by

$$\chi_m = 2 \tan^{-1} \left(\frac{p_c}{b_{\max}} \right) \quad 2-18$$

* Equation 4.66 is

$$S(\chi) = \frac{p_c^2}{(1 - \cos \chi)^2}$$

where $S(\chi)$ is the angular distribution function. The total cross-section is then

$$2\pi \int_0^\pi S(\chi) \sin \chi \, d\chi$$

which results in equation 2-15 if the lower limit is changed from 0 to χ_m .

The impact parameter was chosen to occur with a probability proportional to itself. The deflection angle was then given by

$$\chi = 2 \tan^{-1} \left(\frac{p_c}{b} \right) \quad 2-19$$

2.3.2 The Two Fluid Model For Neutral Plasma Problems

The neutral plasma was considered to be made up of two gases, electron and proton, which were coupled by both their electric fields and their collision interactions. Because two different gases existed, a piston driven into a neutral plasma was not expected to generate a discontinuity that resembled any one Mach number. Instead two discontinuities were expected, one in each gas, with a coupling motion set up between them. This problem could not be called a shock problem but was better described as an impulsively started piston problem.

In order to generate a shock in a hard sphere gas, a piston was driven into it at a velocity given by equation 2-4. This velocity was non-dimensionalized with respect to the most probable velocity of particles in the upstream gas. In a charged particle gas, however, there were two most probable velocities; one for electrons and one for protons. Since the piston could travel at only one velocity it was decided to define an average gas molecule of mass

$$m_g = \frac{m_e + m_p}{2} \quad 2-20$$

The most probable velocity of a gas with this molecular weight was then given by

$$\left(\frac{2 k T}{m_g} \right)^{1/2}$$

All velocities were non-dimensionalized with respect to this value.

If the two gases were completely uncoupled, a piston travelling at Mach 10 with respect to the average gas would set up a Mach 14.068 discontinuity in the proton gas and a Mach 1.18 discontinuity in the electron gas. With two different discontinuities a variation in species density would be set up and in certain regions the plasma would no longer be neutral. An induced electric field was therefore expected.

Within the system each cell was assumed to act as an infinite sheet with respect to its charge distribution. As the field due to an infinite sheet does not vary with distance perpendicular to the sheet, the fields due to each cell are algebraically summable. Outside of the walls this sum is zero since the sum of all charges in the system is zero (i.e. neutral plasma).

The field, E_i , due to a charge distribution, $n_p - n_e$, in a cell was

$$E_i = \pm \frac{e (n_p - n_e) X}{2 \epsilon_0} \quad 2-21$$

where X was the cell width. The $+$ and $-$ specified whether the field was acting at a point to the right or the left of the cell. The total field, F_i , in a cell due to the fields generated by all other cells was

$$F_i = \sum_{j=1}^{i-1} - E_j + \sum_{j=i+1}^{N_c} E_j \quad 2-22$$

where N_c was the number of cells.

Because of the lack of information inherent in the model, the field within a cell due to particles within itself was assumed to be zero. The Monte Carlo method assumed that the model particles represent a much

larger number of actual molecules. For this reason the particles within a cell could not be fixed to one position in order to study fields because each molecule represented many molecules scattered throughout the cell. The minimum resolution of macroscopic properties in the system was, in fact, a cell width. The cell's molecules could be assumed to generate a field within the cell given by equation 2-21, however, there is no method of determining the correct sign (\pm). This question had no answer, and therefore the field was assumed to be zero.

The acceleration on a particle i due to the induced field in a cell j was then

$$a_i = F_j \frac{q_i}{m_i} \quad 2-23$$

This acceleration is the one to be used in equations 2-8 and 2-9.

2.3.3 The Theoretical Resultant Behavior For an Impulsively Started Piston in a Neutral Plasma

It will be constructive to describe at this point the interrelations of the piston-gas reactions, the interparticle reactions, and the electric field-particle reactions from a theoretical point of view.

The physical properties of the resultant system will be due to a physical balance between the three interactions. The general picture has the piston acting as an energy source setting up a flow and density pattern; the electric field attempting to alter flow and density patterns; collisions attempting to communicate energies between directions and between species.

As the piston enters the gas, particles will strike it, reverse their

direction and pick up an added velocity of $13.56 V_{mg}$. At any temperature, the high mass protons have low peculiar velocities and low mass electrons have high peculiar velocities. As a result this added velocity will account for almost all of the protons velocity while the electron gains relatively little added velocity. Since the peculiar velocity of the electrons is much higher than twice the piston velocity, electrons reflected from the piston will move away much faster than the protons. The protons will therefore tend to concentrate near the piston while an electron concentration builds up farther upstream. These two concentrations will act like a dipole and will set up a strong electric field.

The electric field will accelerate electrons toward the piston and protons toward the wall. Consequently, the field will extract flow energy from the electrons and add it to the protons. In the limit the action of the field would destroy itself.

Collisions between particles tend to transfer the extra energy received from the piston into the y and z directions as well as transfer energy between species. On the average they will retard the motion of particles rebounding from the piston by transferring flow energy into thermal energy. The inter-species collisions will have the net result of bringing the temperatures of the two species closer together.

2.3.4 The Time Step Parameter

Since the maximum velocity of the electrons was much higher than that of the protons, the maximum electron velocity was considered in equation 2-10. However, for neutral plasmas, the time step parameter had to be of such a magnitude that it allowed three types of collisions

to occur; electron-electron, electron-proton, and proton-proton. However, the low peculiar velocity of protons made the proton-proton collision frequency considerably less than that of the other two types of collisions. Therefore, the information transfer due to proton-proton collisions was of secondary importance.

The maximum velocity of upstream electrons was approximately $70 V_{mg}$. Since the discontinuity in the electron shock was small, the maximum downstream electron velocity was only approximately $100 V_{mg}$. The proton maximum velocity however was approximately $2 V_{mg}$ in the upstream region and $20 V_{mg}$ in the downstream region. Due to the very weak discontinuity in the electron shock it was assumed for the purpose of determining the time step parameter that the electrons were very nearly in the same state throughout the system. For this condition a time step parameter of a relatively high magnitude did not adversely affect the electron structure since isolation was not extremely critical. It was felt that $S = 5.0$ would not violate the assumptions used to determine the time step parameter for hard sphere gases.* When S was 5.0, the time step parameter based on proton velocities was approximately 1.0. This allowed proton collisions throughout the system, however, most of these collisions were of the proton-electron type. Proton-proton collisions occurred only in the downstream region and in small quantities. It has already been shown that this lack of occurrence was both expected and of little importance.

The presence of the electric field entered into considerations of

* It will be shown in the results that, even for $S = 10$, the results for hard spheres are not in error by more than 10%.

the time step parameter. Since the field acted as a means of dissipating energy in a manner much less effected by the time step parameter than the collisions, it tended to make the time step parameter take on a less important role than it had in the hard sphere case. This was a final consideration which suggested a time step parameter of 5.0 was not too high.

2.3.5 Test Conditions

The neutral plasma was assumed to have an initial temperature of $10,000^{\circ}\text{K}$ (~ 1 eV) and a number density of 10^{15} particles per cubic centimeter. As is generally assumed in theoretical studies of neutral plasmas, the gas was assumed to be 100% ionized and re-association was assumed not to occur.

3. SIMULATION MODEL RESULTS

3.1 The Hard Sphere Gas Model

3.1.1 The Variation of Shock Properties With Time Step Parameter

The simulation model was run for time step parameters of 0.5, 1.0, 1.5, 3.0 and 10.0. From two to four times during each run, complete information about density, temperature, flow, collision frequency, velocity moments and post-collisional velocity moments was printed out. Two or three runs were performed for each time step parameter. Therefore, four or more data sets were available for each time step parameter. These data sets were statistically averaged for each time step parameter to obtain average variations of the properties with position.

The variations obtained in this manner, show very similar behavior. For this reason no graphical presentation was attempted to show the behavior for various time step parameters. Instead, the downstream cell properties were averaged. Between 9 and 11 cells were involved in these averages. The results are shown in Table 1. The last column shows the theoretical upstream values found from standard mass-energy conservation formulae.

From Table 1 it was clear that the properties density, temperature, flow, collision frequency, and velocity moments showed similar accuracies for $S = 0.5$ to $S = 3.0$. All these time step parameters showed errors generally of less than 2% in predicted upstream conditions. For $S = 10.0$ the inaccuracy was much more pronounced, especially for density and collision frequency. The errors for these properties were almost 5%. These results tended to confirm the upper and lower limit analysis presented previously.

The error in the post-collisional velocity moments (i.e. the velocity moments of particles emerging from collision) markedly increased with increasing S . Errors of up to 19% were noted with the best agreement being within 6.5% for $S = 0.5$. These errors however were misleading especially for low values of S . For $S = 0.5$ approximately 20% of the particles have collisions in the downstream region during one time step. Since the velocity moments were found by averaging only over these particles, whereas all other properties average over all particles, post-collisional velocity moments were inherently five times less accurate. When $S = 3.0$ the number of particles averaged over was approximately the same (i.e. approximately every particle had one collision). This would indicate that the best value of S was the smallest value possible. Experimentation, therefore, showed that the value of S should be 0.5.

3.1.2 The Accuracy of the Computer Model

The accuracy of the computer model was tested by three independent means. Firstly, results were compared with the limited experimental results available. Secondly, the model downstream conditions were compared with theoretically derived conditions. Thirdly, the model results were checked to assure that they were consistent within themselves by testing the conservation of mass criteria and the collision frequency variation as described below.

The only experimental results available were shock thicknesses found by electron beam fluorescence techniques. Two different investigations were considered; that of Robben and Talbot² and that of Camac.¹

Robben and Talbot² reported results non-dimensionalized with the

length L^* defined as

$$L^* = \frac{\eta^*}{\rho u} \quad 3-1$$

where η^* was the viscosity at the sonic point and ρu was the flow.

The maximum slope thickness, δ , was defined in the usual manner as

$$\delta = \frac{n_d - n_u}{\left(\frac{dn}{dx}\right)_{\max}} \quad 3-2$$

where n was the number density with d denoting downstream and u denoting upstream. For hard sphere particles the viscosity was defined as

$$\eta^* = \frac{m}{3\sigma} \left(\frac{8 k T^*}{\pi m} \right)^{1/2} \quad 3-3$$

where m was the molecular weight of the gas. Equation 3-1 then reduce to

$$\frac{L^*}{\delta} = \frac{1}{3 \delta n \sigma M} \left(\frac{8}{\pi \gamma} \frac{(2 + (\gamma - 1) M^2)}{\gamma + 1} \right)^{1/2} \quad 3-4$$

since

$$\rho u = m n M \left(\frac{\gamma k T}{m} \right)^{1/2} \quad 3-5$$

and

$$\frac{T^*}{T} = \frac{2 + (\gamma - 1) M^2}{\gamma + 1} \quad 3-6$$

The problem was to determine what molecular radius should be assumed in order to determine the cross-section σ . Rather than assume a radius it was decided to use the maximum slope thickness determined by the Monte Carlo simulation model and use equation 3-4 with the Robben and Talbot² results to predict molecular radii.

Robben and Talbot² reported L^*/δ values between .141 and .17 for Mach 10.0 shocks in argon, helium and nitrogen. The Monte Carlo model predicted a thickness of 1.22×10^{-3} cm. The corresponding molecular radii would be 0.98×10^{-8} cm to 0.90×10^{-8} cm.

Camac¹ reported shock thicknesses non-dimensionalized with upstream mean free path. For hard spheres this ratio was given by

$$\frac{\lambda}{\delta} = \frac{0.707}{\delta n \sigma} \quad 3-7$$

The experimental values reported ranged from 0.181 to 0.245 for Mach 10.0 shocks in argon. Solving equation 3-7 for molecular radii, values ranging from 1.59×10^{-8} cm to 1.37×10^{-8} cm were obtained.

Table 2 shows some typical molecular radii estimated from viscosity data at 0°C. The values range from approximately 1.1×10^{-8} cm to 1.9×10^{-8} cm. The radii predicted by Camac's¹ results fall roughly in the middle of this range. Robben and Talbot's² results predicted radii slightly below this range.

A detailed error analysis for the downstream conditions was performed for $S = 0.5$. The reference datum was the theoretically calculated conditions. Table 3 shows the results. The first column gives the percentage error while the second column shows the predicted value divided by the theoretical value.

The two most important properties, the density and temperature ratios, agreed to within 2%. The flow was exact to two decimal points! The collision frequency was accurate to within 1%. The velocity moments were in error by approximately 4%. The maximum error occurred for the primary velocity moment of particles emerging from collision. However, the error

was still less than 7% and this error has already been shown to be inherently 5 times greater than other errors. Overall the Monte Carlo model conditions were very close to the theoretical values.

Two checks were possible to ensure that the simulation model gave results which were consistent within themselves. Firstly, conservation of mass required that the mass flow rate (product of density and flow at any position) should be a constant. Secondly, the collision frequency should vary as $n\sqrt{T}$. Table 4 shows a check on the mass flow rate. The maximum error occurs at a point roughly two-thirds of the way through the shock. This maximum error was less than 4% which is small.

Figure 2 shows the collision frequency structure as given by the Monte Carlo simulation. The points plotted are those found by multiplying the upstream collision frequency by

$$\frac{n_x \sqrt{T_x}}{n_u \sqrt{T_u}}$$

where x denotes the position in the shock and u denotes the upstream values. The temperature and density used were those predicted by Monte Carlo simulation. It may be seen that the two predictions agreed very well.

Confidence in the method was therefore established in three different ways. Comparison with experimental results was shown to be favourable. Theoretically expected values were obtained to a very good tolerance. Finally, it was shown that the results were consistent within itself. The present Monte Carlo simulation model therefore was found to be a good workable approximation to the real shock wave behavior.

3.1.3 The Shock Structure

Figures 3 through 10 show the shock structure of various properties for $S = 0.5$. The curves were visually fitted through data points which were obtained by statistically averaging six data sets. The scatter is very small on all graphs except for the collision frequency and the post-collisional velocity moments. It has already been shown in Section 3.1.1 that less accuracy and more scatter was expected in the post-collisional velocity moments due to sample size. The same type of argument may be used to explain the collision frequency scatter. The collision frequency, ν , was calculated by the formula

$$\nu = \frac{2 N_k}{N \Delta t} \quad 3-8$$

where N was the number of particles and N_k was the number of collisions in the time step Δt . The average was therefore, over the number of collisions per particle per time step which was a number less than one. There was therefore less data available for the collision frequency than for a property such as density. However, it has already been shown that the collision frequency structure agrees very well with that predicted by the pressure and temperature structures.

The upstream equilibrium lines shown on Figures 3 through 10 are the theoretical and not the values shown in Table 1. The data points emphasize how well the model predicts these theoretical upstream properties.

A curious anomaly manifested itself in the primary post-collisional velocity moment structure. The values first overshoot then returned to approximately the downstream value of 16.06. This behavior is shown by a solid line. However, very soon after the curve returned to the downstream

value it rose once more and peaked a second time. Comparing this curve to the other shock structures it was seen that at the point where the shock first returns to its downstream value all the other properties had also reached their downstream values. In other words, the second peak occurred somewhere in the region behind the shock. The reason for its occurrence probably lies in interference with the piston. Since the number of model molecules was very much lower than the total number of actual molecules and since high speed molecules tended to collide more frequently, molecules that had rebounded from the piston dominated the collision model in the first few cells.

Figure 11 shows the post-collision velocity moment as predicted by two individual data sets. The anomaly described above is clearly shown as is the initial return to the downstream conditions. The solid line is identical to that in Figure 9.

In the region of major interest, that through the shock, the structure was acceptable. Any inaccuracies may be reduced by rerunning the program to obtain more data for a better statistical average.

The new Monte Carlo simulation model, therefore, produces very reasonable looking results with very low scatter for a small sample size.

3.1.4 A Comparison of the Presented Monte Carlo Model to Other Monte Carlo Models

Mach 10 results for two other Monte Carlo simulation studies were available; those of Bird⁵ and those of Macpherson.⁷ Both of these models were more limited than the present model in that they did not allow for varying interaction cross-sections. In this respect the new model was much more general with direct applications to multi-component gases.

Bird's⁵ results show that the shock thickness parameter, λ/δ , should be 0.31 which suggested a shock which is definitely too thin when compared with experimental results. This could, however, be caused by assuming an inaccurate molecular radius when calculating λ . The longitudinal temperature overshoot seen in Figure 7 was also observed by Bird⁵. His maximum value was approximately $20 V_m^2$ while the present model predicted approximately $21 V_m^2$. The theory of Yen¹⁹ predicted a maximum temperature overshoot of $21 V_m^2$, therefore, the new Monte Carlo simulation is marginally closer than Bird's⁵ model.

Macpherson's⁷ results showed a maximum slope thickness of 1.33×10^{-3} cm. This agrees well with the present value of 1.22×10^{-3} . The longitudinal temperature overshoot was $21.5 V_m^2$ in Macpherson's⁷ work which once more agrees well with the present work.

3.2 The Neutral Plasma Model

It was a great disadvantage that no experimental data or even sound theoretical information was available with which to compare the neutral plasma model. The results were compared with the logically expected behavior.

Figure 12 shows electron and proton density profiles. The two separate concentrations are clearly visible. Near the piston the proton density greatly exceeded the electron density. At approximately 1.9×10^{-4} cm a neutral plasma position occurred. From here to the shock foot an electron concentration existed.

Figure 13 shows the electric field in the system. When the particle field was initially set up, random positioning placed different numbers of each species in each cell. This in turn set up an electric field

which will be referred to as noise. The magnitude of this noise is shown as a dashed line in Figure 13. The electric field in Figure 13 was very well defined. It went to zero as expected at both extremes. Comparing Figures 12 and 13, the field has values of the same magnitude as the noise field at approximately the electron shock foot. The field maximum occurs at 1.9×10^{-4} cm which is the neutral plasma point. It was at this point that maximum particle acceleration occurred.

Figure 14 shows the proton and electron temperature profiles. An average shows the downstream temperatures to be 61.3 and 1.34 for protons and electrons respectively. In Section 2.3.2 it was shown that if the gases were uncoupled, two discontinuities would result. The downstream temperatures of these uncoupled discontinuities would be 62.7 and 1.17 for protons and electrons respectively. Collision coupling of the two gases, therefore, must have occurred since the temperatures have moved toward an equilibrium. The electron temperature had too small a magnitude to show abnormalities. The proton temperature however, shows a definite overshoot. The position of this overshoot was 1.9×10^{-4} cm which corresponded to the neutral plasma point. This would suggest that the two features are correlated.

Figure 15 shows the proton and electron flow profiles. The proton flow was of a high magnitude. This was due to the influence of the piston and the fact that the electric field accelerates the protons negatively. The electron flow, however, was retarded by the field and was less affected by the piston due to the high peculiar velocity of electrons. Since the electrons were much lighter than protons, equation 2-23 shows that electron accelerations were much higher than proton

accelerations. The combined effects keep the electron flow very low.

The behavior of the model was clearly consistent with the logically expected behavior. The electron behavior, except in regard to densities, exhibited very little departure from the initial state. The proton behavior showed gross departures from the initial state as was logically expected. The model remained stable at all times.

PART II

THE BOLTZMANN EQUATION

4. THE BOLTZMANN EQUATION AND IT'S SOLUTION

For any species in a gas the Boltzmann equation is written as

$$\frac{\partial f}{\partial t} + \underline{c} \cdot \frac{\partial f}{\partial \underline{r}} + \underline{a} \cdot \frac{\partial f}{\partial \underline{c}} = \left(\frac{\partial f}{\partial t} \right)_{\text{col}} \quad 4-1$$

where f is the velocity distribution function, t is the time, \underline{c} is the molecular velocity, \underline{a} is the acceleration due to external fields, and the right hand side is the collision term. The rigorous form of the collision term is

$$\int_0^{\infty} \int_0^{2\pi} \left(f'_1 f'_2 - f_1 f_2 \right) g b db d\eta$$

where g is the relative speed, b is the impact parameter and η is the angle specifying the orientation of the plane of relative orbits. The subscripts denote the two collision partners and the (') denotes conditions after collision. Except for simple cases, such as steady state, this form is unsolvable.

In recent years many authors including Krook¹⁴, Anderson¹⁵ and Holway¹⁶ have used a statistical model of the form

$$v(\psi - f)$$

to represent the collision term. Here v is the collision frequency and ψ is the distribution of velocities of molecules that have just undergone a collision. Holway¹⁶ went on to show that ψ was given by the relationship

$$\psi = (2\pi)^{-\frac{3}{2}} \left| \underline{\lambda} \right|^{-\frac{1}{2}} \exp - \frac{1}{2} \left[\epsilon_{ij} (c_i - u_i) (c_j - u_j) \right] \quad 4-2$$

where $\underline{\lambda}$ is the second order velocity moment matrix of molecules emerging from collision and $\underline{\varepsilon}$ is its tensor inverse. The flow is denoted by \underline{u} .

For a steady one-dimensional shock wave in a single component gas with no external field, Appendix II shows that the Boltzmann equation may be represented by the three equations

$$c_1 \frac{\partial f_1}{\partial r_1} = v \left(\psi_1 - f_1 \right) \quad 4-3a$$

$$f_2 = \psi_2 \quad 4-3b$$

$$f_3 = \psi_3 \quad 4-3c$$

where ψ_1 , ψ_2 , and ψ_3 , f_1 , f_2 , and f_3 are the component equations of ψ and f respectively. The component equations of ψ are derived in Appendix III.

The finite difference form of equation 4-3a is

$$\Delta f = \frac{v}{c_1} (\psi_1 - f_1) \Delta r \quad 4-4$$

and a finite difference solution for f at any point, n , is

$$f_1^n = f_1^0 + \frac{v}{c_1} \left(\psi_1^n - f_1^{n-1} \right) \Delta r \quad 4-5$$

where f_1^0 is the original value of f_1 . For any value of c_1 equation 4-5 may be solved for f_1 at any point. This equation therefore, provides a means of solving the Boltzmann equation at a number of velocity and spacial points. The resultant field may then be fitted with a bi-cubic spline.

A spline is a piece-wise continuous curve fitting technique. It is

based on fitting a third order polynomial between any two points such that at each of the points the first and second derivatives are continuous. By supplying a set of data points consisting of a set of abscissa points (x) with the corresponding ordinate points (y) and by specifying the boundary conditions at the extremes, a simple cubic spline may be fitted to the data points. This spline has the following properties. It passes smoothly through each point provided. Between data points the curve is continuous. The first and second derivatives at the data points are continuous.

The above description may be extended to a bi-cubic spline where the values to be fitted are functions of two variables (eg. z as a function of x and y). In this case a surface is fitted to a grid system. The surface will be smooth with the first and second derivatives at points along grid boundaries being continuous. Within each grid the surface is continuous and smooth.

The cubic spline fit provides a method of expressing y as a function of x in the form

$$y = a_{1n} + a_{2n} x + a_{3n} x^2 + a_{4n} x^3 \quad 4-6$$

where the n denotes the cell number along the x axis (i.e. the given data points divide the x axis into a number of cells) for the bi-cubic spline z is expressed by

$$\begin{aligned} z = & a_{1mn} + a_{2mn} x + a_{3mn} x^2 + a_{4mn} x^3 \\ & + a_{5mn} y + a_{6mn} xy + a_{7mn} x^2 y + a_{8mn} x^3 y \\ & + a_{9mn} y^2 + a_{10mn} x y^2 + a_{11mn} x^2 y^2 + a_{12mn} x^3 y^2 \end{aligned}$$

(over)

$$+ a_{13mn} y^3 + a_{14mn} x y^3 + a_{15mn} x^2 y^3 + a_{16mn} x^3 y^3 \quad 4-7$$

(Price²⁰) where m denotes the y cell and n denotes the x cell.

The values of the \underline{a} matrix are found by methods described by Ahlberg, Nilson and Walsh²¹.

It is immediately apparent that once the z -grid is defined the value of z at any point within the defined boundaries of x and y is immediately obtainable. It is seen that by finding the distribution function at a finite number of points in c_1 and r_1 , a bi-cubic spline may be fitted to the resulting grid in order to complete the solution.

By solving the finite difference equation, 4-5, for a number of c_1 values at a number of spacial points, r_1 , a grid system was generated. The spline then completed the solution.

The finite difference evaluation of f_1 was simplified by the use of simple cubic splines. To evaluate equation 4-5 the value of v and ψ_1 must be known at any point. Monte Carlo simulation studies gave v directly at a number of points in the shock. The distribution function ψ_1 is derived in Appendix III as

$$\psi_1 = \left(2\pi (\epsilon_{22} \epsilon_{33} - \epsilon_{23}^2) |\underline{\lambda}| \right)^{-\frac{1}{2}} \exp - \frac{v_1^2}{2} \left(\epsilon_{11} - \frac{\epsilon_{12}^2 \epsilon_{33} + \epsilon_{13}^2 \epsilon_{22} - 2 \epsilon_{12} \epsilon_{13} \epsilon_{23}}{\epsilon_{22} \epsilon_{33} - \epsilon_{23}^2} \right) \quad 4-8$$

where $\underline{\lambda}$ is the moment matrix of particles emerging from collision and $\underline{\epsilon}$ is its tensor inverse. In the Monte Carlo simulation there was no evidence to indicate that λ_{12} , λ_{13} or λ_{23} were other than zero.

Equation 4-8 will therefore reduce to

$$\psi_1 = \left(2 \pi \lambda_{11} \right)^{-1/2} \exp - \frac{v_1^2}{2 \lambda_{11}} \quad 4-9$$

This form bears a strong resemblance to Krook's¹⁴ equation for ψ_1 which is

$$\psi_1 = \left(2 \pi \bar{c}_1^2 \right)^{-1/2} \exp - \frac{v_1^2}{2 \bar{c}_1^2} \quad 4-10$$

where \bar{c}_1 is defined as

$$\bar{c}_1 = \left(\frac{k T}{m} \right)^{1/2} \quad 4-11$$

The quantity \bar{c}_1^2 is therefore the velocity moment corresponding to the local kinetic temperature. Except under equilibrium conditions \bar{c}_1^2 will not equal λ_{11} . The Holway¹⁶ model is therefore a refinement of the original Krook¹⁴ expression.

Expressing equation 4-9 in the form

$$\psi_1 = a(r) \exp - b(r) v_1^2 \quad 4-12$$

it can be seen that equation 4-5 may be evaluated once $v(r)$, $a(r)$, $b(r)$, and $u_1(r)$ are obtained. The flow $u_1(r)$ is necessary in order that v_1 may be found at any position given the molecular velocity c_1 . The variation of these quantities was obtained by fitting simple cubic splines to the values of v , a , b and u_1 given by the Monte Carlo simulation study. It was found that twenty data points were more than sufficient for this purpose.

5. DISCUSSION OF RESULTS

Once the splines are defined for the variation of v and ψ_1 , equation 4-5 may be evaluated using any desired value of Δr . It was found that for $\Delta r < 0.2 \times 10^{-5}$ cm the numerical integration yielded similar results. Equation 4-5 was then used to define a field for twenty values of r_1 and sixty-five values of c_1 . This field was then fitted with a bi-cubic spline which completed the solution.

The accuracy of the distribution functions found by the finite difference evaluation was tested by comparing the variation of the primary velocity moment obtained by integration, with that obtained directly from the simulation study. As a second test, Krook's¹⁴ formulation of ψ_1 was used.

Figure 16 compares the Monte Carlo results with the integration results of both ψ_1 formulations. Near the foot of the shock both formulations show poor agreement. This is primarily attributed to the insensitivity of the statistical model of the collision term and to the inaccuracy of Monte Carlo data near the foot of the shock. It has been shown in Section 3 that the accuracy of the post-collisional velocity moments is much poorer than that for other properties. Since the Krook¹⁴ formulation is based on temperature, the error of its prediction depended much less on the Monte Carlo process than that for Holway's¹⁶ formulation. It is significant therefore, that Holway's¹⁶ formulation shows much better correlation with observed behavior away from the shock foot. Especially of note is the prediction of the magnitude and position of the overshoot. Holway's¹⁶ maximum overshoot is only slightly behind the observed overshoot while the Krook¹⁴ overshoot occurs much later. This figure convincingly shows

that Holway's¹⁶ formulation is superior to that of Krook.¹⁴

Figures 17 through 21 show the distribution functions at various positions in the shock as predicted by Holway's¹⁶ formulation. The upstream and downstream distributions are perfectly maxwellian. The intermediate states at $x = 2.8 \times 10^{-3}$ cm and $x = 3.6 \times 10^{-3}$ cm show the upstream peak rapidly shrinking while the upstream maxwellian grows out to the left. At $x = 4.4 \times 10^{-3}$ cm the longitudinal temperature is near the top of its overshoot. The distribution is seen to be very nearly maxwellian about the local longitudinal temperature. From this point to the downstream position, the distribution simply shifts to its proper velocity position and perfects its maxwellian nature.

A comparison of the secondary velocity moment is shown in Figure 22. It has been shown in Appendix II that for hard sphere molecules

$$f_2 = \psi_2 \quad 5-1$$

This implied that the variation of the secondary velocity moment of molecules emerging from collision is the same as the secondary velocity moment at the position. The Holway¹⁶ formulation therefore, is represented by the post-collisional secondary velocity moment. The Krook¹⁴ formulation arises from equation 4-10. It is seen that both the Krook¹⁴ and Holway¹⁶ formulations show the same size of error. However, in order to gain accurate distribution functions at any point in the 2 and 3 directions, equation 5-1 shows that

$$f_2 = (2\pi M_{22})^{-1/2} \exp \left(-\frac{1}{2} v_2^2 / M_{22} \right) \quad 5-2$$

where M_{22} is the secondary velocity moment value at the point. Due to

symmetry f_3 is equal to f_2 .

The present approach used to solve Boltzmann's equation is much less complicated numerically than the methods used by Anderson¹⁵ and other numerical experimenters. It also has the advantage of remaining at all times dependent on physical behavior patterns rather than numerical convergence criteria. The application of the spline fit allows a complete solution to be obtained.

PART III

CONCLUDING REMARKS

6. CONCLUDING REMARKS

The impulsively started piston problem has been solved by a new and more general Monte Carlo model of molecular behavior. The model was based on the time of collision free flight given by Denisik et al¹⁷ and assumed that the behavior of a gas was predicted by the behavior of a subgroup of the gas molecules. Two gases were modeled, one composed of "hard sphere" molecules the other of equal numbers of electrons and protons. The model was solved by means of an IBM 360-65 computer.

The impulsively started piston in the "hard sphere" gas produced a shock wave. The resulting shock wave structure was used to solve the Boltzmann equation in the BGK formulation. The impulsively started piston in the neutral plasma demonstrated that the new model could be applied to a gas for which the collision cross-section was not a constant but a function of the initial conditions of the colliding particles.

In Section 2.1 it was shown that the new Monte Carlo model was more general and exact than the previous models. This conclusion was based on three considerations. Firstly, the randomness of collisions was inherently considered. Secondly, collisions with all other particles are considered in the formulation. Finally, collisions whose interaction cross-sections are not constant could be treated.

In Section 3.1.2 the results of the Monte Carlo model as formulated for hard sphere molecules were tested to prove their accuracy. The shock thicknesses predicted by the model compared very well with the experimentally derived results of Camac¹ and less well with those of Robben and Talbot². The downstream conditions as derived by the model agreed with the results predicted by continuum theory. Both the

conservation of mass law and the collision frequency were verified accurately.

In section 3.2 the results of the impulsively started piston in a neutral plasma were demonstrated to agree with logically expected behavior.

The solution of the Boltzmann equation given in Sections 4 and 5 were obtained in a very simple, straight forward manner. A comparison of longitudinal velocity moments predicted by the Monte Carlo model and the Boltzmann equation solution showed only fair agreement. However, the Holway formulation of the post-collisional velocity distribution yielded a more accurate indication of these moments than did the Krook formulation.

The new Monte Carlo model in the charged-particle formulation has several applications as discussed below. However, four extensions are necessary before these realistic problems can be attempted.

The most important extension would be the consideration of the association of ions and electrons. This could be achieved by a consideration of the energy of collision and the ionization potential. Furthermore, re-ionization of the resulting neutral products of association could be considered in the same manner. This extension would allow studies of problems where 100% ionization cannot be assumed.

The consideration of radiation effects would be a second extension. Both bremsstrahlung and cyclotron radiation could be considered. Since the former type of radiation is a collision phenomenon, the Monte Carlo method is especially well suited to its study.

Two simpler extensions would be the consideration of external

electromagnetic fields and the treatment of relativistic electrons. Both these extensions may be based on well known equations of behavior.

As was stated in the introduction, the basic mechanisms of importance in ionized gas problems are well understood. The power of the Monte Carlo method lies in the fact that it allows these well understood mechanisms to be used in complex situations to predict plasma behavior. Three problems that could be treated in this manner will be described.

The gas discharge tube has been exhaustively studied yet still presents several unsolved problems.²² The modeling of a gas discharge tube would be a good problem to consider while developing the Monte Carlo model techniques. The available experimental information (contained in such works as Howatson²³) would furnish an excellent comparison for Monte Carlo results. By this comparison, both the model itself and the computational techniques involved in its solution could be refined.

It is a well known fact that a plasma will reflect and not transmit electromagnetic waves whose frequency is below the plasma frequency. This causes a resonance in the electromagnetic wave at the plasma frequency. Experiments with a gas discharge tube inside a wave guide confirm this resonance but also indicate several other resonances.²² It has been theorized that this multiple resonance is due to non-uniform electron density. The confirmation of this theory is within the scope of the Monte Carlo simulation model. With the model, a detailed study of the microscopic interaction of the plasma and the wave could be performed.

Thermonuclear fusion power generation experimentation is a very costly undertaking--not to mention the danger involved to life and

property. At present a great deal of work centers around finding equipment geometry that will contain a plasma at high pressures and temperatures. However, due to plasma instabilities all designs to date have failed.²⁴ It should be possible to construct a Monte Carlo model of the plasma in the thermonuclear range and use this model to perform computer simulations of proposed equipment configurations. In this manner, the feasibility of a design could be ascertained in a relatively inexpensive and absolutely safe way.

A third problem that could be studied by a Monte Carlo model is that of coronal heating. The manner in which the energy of the sun is passed from the photosphere to the chromosphere and corona is not known.²² The best theory to date proposes a mechanism involving acoustic and shock waves generated in the photosphere and propagating through to the corona. At present it is impossible to make close range studies of behavior on the surface of the sun. The Monte Carlo model could provide a method of obtaining both an understanding of the mechanisms involved and a testing of the proposed theories.

The three preceding studies were chosen to demonstrate the versatility of the Monte Carlo method. The first study provides confirmation of an existing theory. The second study provides an inexpensive method of performing feasibility study of thermonuclear problems. The third study provides a means of obtaining information in a situation where direct observation is hampered by extraordinary circumstances.

As a research tool in the study of plasma physics, the Monte Carlo modeling technique offers a unique advantage. Since the programming of the model is at all times under the control of the researcher, the

inclusion of any particular mechanism, such as collisions, radiation, etc., is decided by him. This allows the contribution of any particular mechanism to be directly evaluated--an evaluation which is generally very difficult with laboratory experiments.

It is concluded that the Monte Carlo method constructed under the new formulation provides a powerful tool for the investigation of gas dynamic problems.

REFERENCES

1. Camac, M., "Argon Shock Structure", *Rarified Gas Dynamics* (1960), Vol. 2, pp.240-249.
2. Robben, F. and Talbot, L., "Measurement of Shock Wave Thickness by the Electron Beam Fluorescence Method", *Physics of Fluids*, Vol. 9, Num. 4, 1966, pp. 633-643.
3. Shapiro, A. H., "The Dynamics and Thermodynamics of Compressible Fluid Flow", The Ronald Press Company, New York, 1953.
4. Bird, G. A., "The Velocity Distribution Function within a Shock Wave", *JFM*, Vol. 30, Part 3, (1967), pp. 479-487.
5. Bird, G. A., "Shock Wave Structure in a Rigid Sphere Gas", *Rarified Gas Dynamics* (1965), Vol. 1, pp. 216-222.
6. Bird, G. A., "The Formation and Reflection of Shock Waves", *Rarified Gas Dynamics* (1959), pp. 301-311.
7. Macpherson, A. K., "Shock Collision at a Molecular Level", *JFM*, Vol. 39, Part 4, 1969, pp. 849-861.
8. Macpherson, A. K., "Rotational Temperature Profiles of Shock Waves in Diatomic Gases", unpublished.
9. Sutton, G. W. and Sherman, A., Engineering Magnetohydrodynamics, McGraw-Hill Book Company, New York, 1965.
10. Holt, E. H. and Haskell, R. E., Foundations of Plasma Dynamics, The Macmillan Company, New York, 1965.
11. Chapman, S. and Cowling, T. G., The Mathematical Theory of Non-Uniform Gases, Third Edition, Cambridge, Cambridge, 1970.
12. Mott-Smith, H. M., "The Solution of the Boltzmann Equation for a Shock Wave", *Physical Review*, Vol. 82, Num. 6, 1951, pp. 885-892.
13. Bhatnagar, P. L., Gross, E. P., and Krook, M., "A Model for Collision Processes in Gases. I. Small Amplitude Processes in Charged and Neutral One-Component Systems", *Physical Review*, Vol. 94, Num. 3, 1954, pp. 511-525.
14. Krook, M., "Dynamics of Rarified Gases", *Physical Review*, Vol. 99, Num. 6, 1955, pp. 1896-1897.
15. Anderson, D. G., "Numerical Solutions of the Krook Kinetic Equation", *JFM*, Vol. 25, Part 2, 1966, pp. 271-287.
16. Holway, L. H., Jr., "New Statistical Models for Kinetic Theory: Methods of Construction", *The Physics of Fluids*, Vol. 9, Num. 9, 1966, pp. 1658-1673.

17. Denisik, S. A., Malama, Y. G., Polak, L. S., and Rezvanov, R. A., "Application of the Monte Carlo Method in the Solution of Some Problems of Physical and Chemical Kinetics", *Teplofizika Vysokikh Temperatur*, Vol. 5, Num. 6, pp. 1011-1017.
18. Bird, G. A., "Aerodynamic Properties of Some Simple Bodies in the Hypersonic Transition Regime", *AIAA Journal*, Vol. 4, No. 1, 1966, pp. 55-60.
19. Yen, S-M, "Temperature Overshoot in Shock Waves", *Physics of Fluids*, Vol. 9, No. 7, 1966, pp. 1417-1418.
20. Price, G. V., Master's Thesis, University of Manitoba, 1972.
21. Ahlberg, J. H., Nilson, E. N., and Walsh, J. L., The Theory of Splines and Their Applications, Academic Press, New York, 1967.
22. Boley, F. I., Plasmas-Laboratory and Cosmic, D. Van Nostrand Company, Inc., Princeton, 1966.
23. Howatson, A. M., An Introduction to Gas Discharges, Pergamon Press, Oxford, 1965.
24. Glasstone, S. and Lovberg, R. H., Controlled Thermonuclear Reactions, D. Van Nostrand Company, Inc., Princeton, 1960.
25. Jeans, J., An Introduction to the Kinetic Theory of Gases, Cambridge, Cambridge, 1967.

TABLES AND FIGURES

TABLES AND FIGURES

- TABLE 1 Summary Of Downstream Shock Properties For Varying Time Step Parameter(s) as Compared to the Theoretical
- TABLE 2 Some Typical Molecular Radii
- TABLE 3 Error Analysis For Time Step Parameter of 0.5
- TABLE 4 Percent Error in Conservation of Mass Requirement
- FIGURE 1 THE MODEL SYSTEM
- FIGURE 2 COMPARISON OF OBSERVED COLLISION FREQUENCY WITH THEORETIC
- FIGURE 3 DENSITY VARIATION WITH POSITION
- FIGURE 4 TEMPERATURE VARIATION WITH POSITION
- FIGURE 5 FLOW VARIATION WITH POSITION
- FIGURE 6 COLLISION FREQUENCY VARIATION WITH POSITION
- FIGURE 7 PRIMARY VELOCITY MOMENT VARIATION WITH POSITION
- FIGURE 8 SECONDARY VELOCITY MOMENT VARIATION WITH POSITION
- FIGURE 9 POST-COLLISIONAL PRIMARY VELOCITY MOMENT VARIATION WITH POSITION
- FIGURE 10 POST-COLLISIONAL SECONDARY VELOCITY MOMENT VARIATION WITH POSITION
- FIGURE 11 POST-COLLISIONAL PRIMARY VELOCITY MOMENT VARIATION AS PREDICTED BY TWO INDIVIDUAL DATA SETS
- FIGURE 12 DENSITY PROFILES FOR ELECTRONS AND PROTONS
- FIGURE 13 ELECTRIC FIELD VARIATION
- FIGURE 14 TEMPERATURE PROFILES FOR ELECTRONS AND PROTONS
- FIGURE 15 FLOW PROFILES FOR ELECTRONS AND PROTONS
- FIGURE 16 COMPARISON OF THE PRIMARY VELOCITY MOMENTS PREDICTED BY THE SIMULATION MODEL WITH THOSE PREDICTED BY THE INTEGRATION OF THE BOLTZMANN EQUATION USING HOLWAY'S FORMULATION AND KROOK'S FORMULATION

- FIGURE 17 DISTRIBUTION FUNCTION, f_1 , AT $r_1 = 2.0 \times 10^{-3}$ cm
- FIGURE 18 DISTRIBUTION FUNCTION, f_1 , AT $r_1 = 2.8 \times 10^{-3}$ cm
- FIGURE 19 DISTRIBUTION FUNCTION, f_1 , AT $r_1 = 3.6 \times 10^{-3}$ cm
- FIGURE 20 DISTRIBUTION FUNCTION, f_1 , AT $r_1 = 4.4 \times 10^{-3}$ cm
- FIGURE 21 DISTRIBUTION FUNCTION, f_1 , AT $r_1 = 5.2 \times 10^{-3}$ cm
(downstream position)
- FIGURE 22 COMPARISON OF HOLWAY, KROOK, AND MONTE CARLO PREDICTIONS
FOR SECONDARY VELOCITY MOMENT

TABLE 1

Summary of Downstream Shock Properties For Varying Time Step
Parameters(S) as Compared to the Theoretical

Property	S	0.5	1.0	1.5	3.0	10.0	Theory
Non-Dimensional Density		3.91	3.89	3.92	3.90	3.67	3.88
Non-Dimensional Temperature		31.56	31.61	31.88	31.07	32.47	32.12
Flow (u_1/V_m)		-6.78	-6.79	-6.79	-6.74	-6.88	-6.78
Collision Fre- quency ($\times 10^{-3}/\text{sec}$)		43.78	44.98	44.19	44.63	41.63	44.14
Primary Velocity Moment (v_1^2/V_m^2)		16.37	15.47	16.17	15.94	16.20	16.06
Secondary Velocity Moment (v_2^2/V_m^2)		15.35	15.97	15.80	15.5	16.12	16.06
Post-Collisional Primary Velocity Moment (v_1^2/V_m^2)		17.09	17.74	19.01	18.99	18.81	16.06
Post-Collisional Secondary Velocity Moment (v_2^2/V_m^2)		15.35	18.40	17.86	18.40	18.88	16.06

TABLE 2

Some Typical Molecular Radii At 0° Centigrade

Gas	Radius (cm)
Helium	1.09×10^{-8}
Neon	1.30×10^{-8}
Argon	1.83×10^{-8}
Hydrogen	1.38×10^{-8}
Nitrogen	1.89×10^{-8}

(From: "An Introduction to the Kinetic Theory of Gases" by James Jeans, p. 183).

TABLE 3

Error Analysis For Time Step Parameter of 0.5

Property	% Error	Ratio of Measured to Theoretic
Density Ratio	0.77	1.01
Temperature Ratio	-1.74	0.98
Upstream Flow	0	1.00
Upstream Collision Frequency	-0.81	0.99
Primary Velocity Moment	+1.93	1.02
Secondary Velocity Moment	-3.80	0.96
Primary Velocity Moment (Post-Collisional)	+6.40	1.06
Secondary Velocity Moment (Post-Collisional)	+2.68	1.02
Shock Propagation Speed	+0.22	1.00

TABLE 4
Percent Error in Conservation of Mass Requirement

Position ($\times 1000$ cm)	Flow	Error (%)
3.0	9.13	0
3.5	9.13	0
4.0	9.21	.9
4.5	9.27	1.5
5.0	9.22	1.0
5.5	8.79	-3.8
6.0	8.99	-1.6
6.5	9.11	-.2
7.0	9.11	-.2

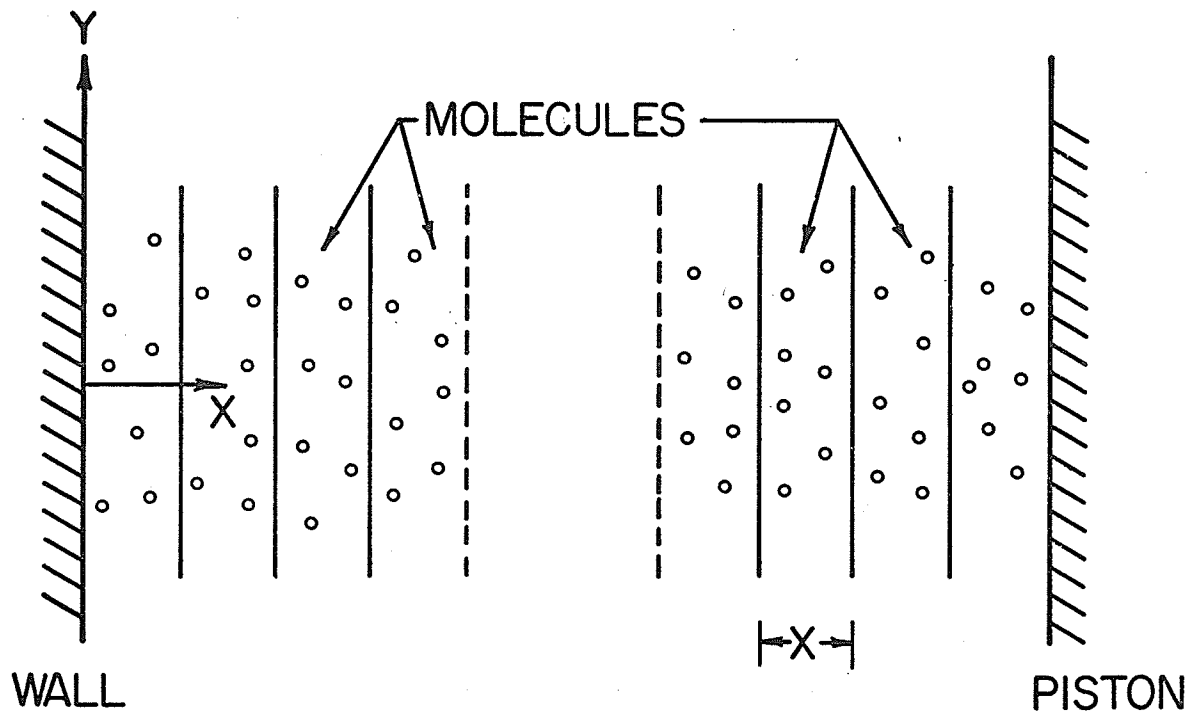


FIGURE I THE MODEL SYSTEM

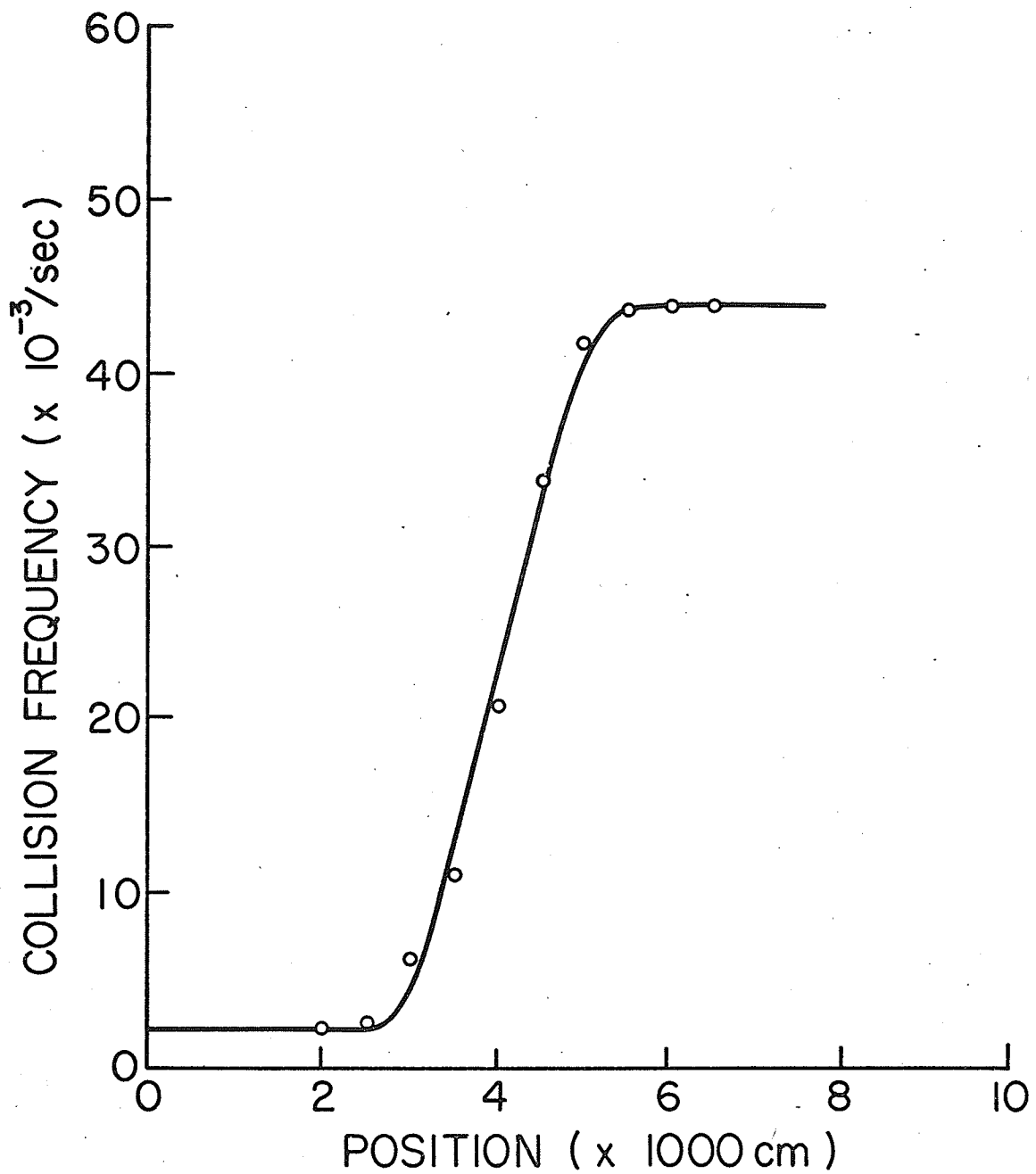


FIGURE 2 COMPARISON OF OBSERVED COLLISION FREQUENCY WITH THEORETIC

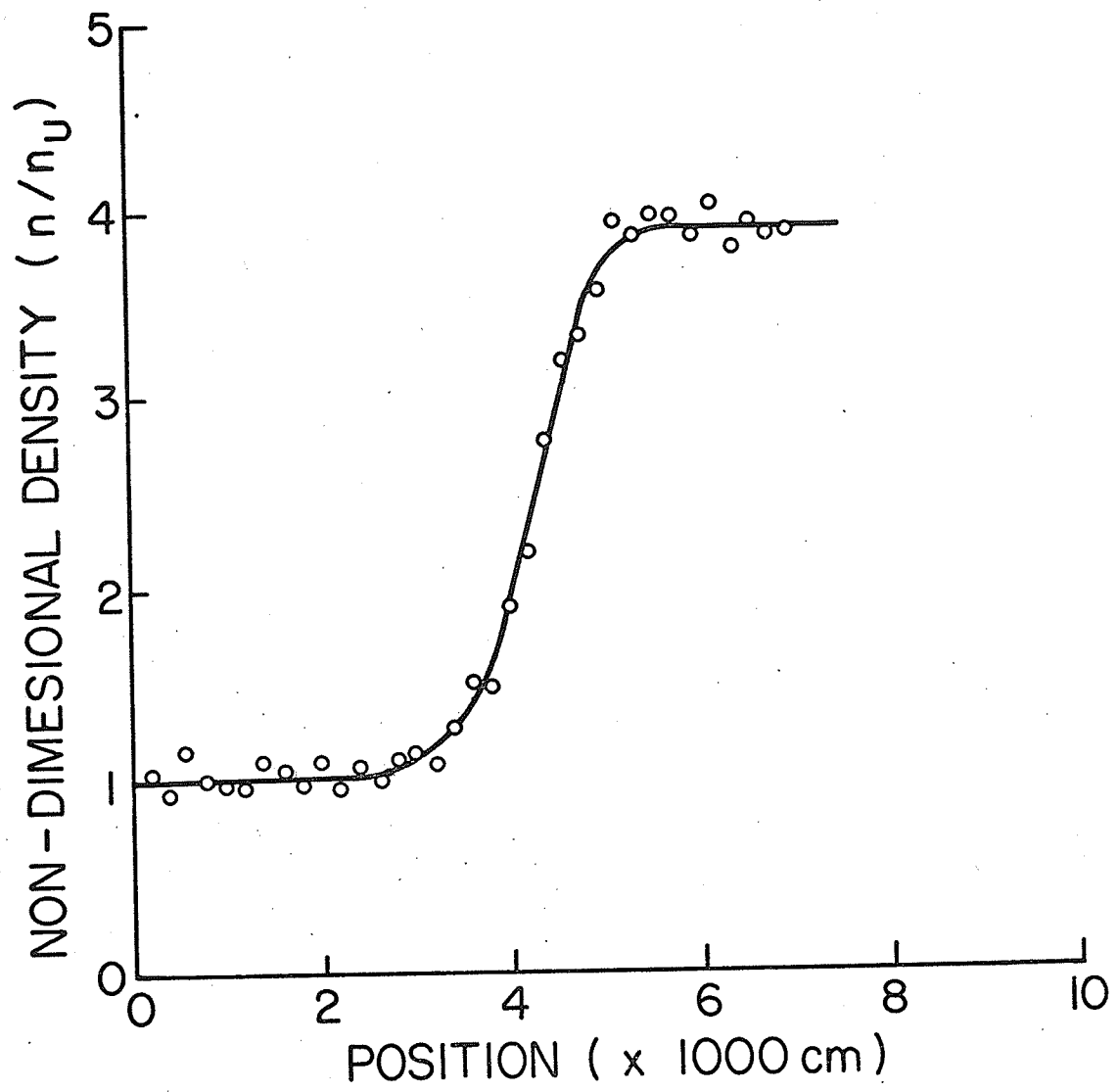


FIGURE 3 DENSITY VARIATION WITH POSITION

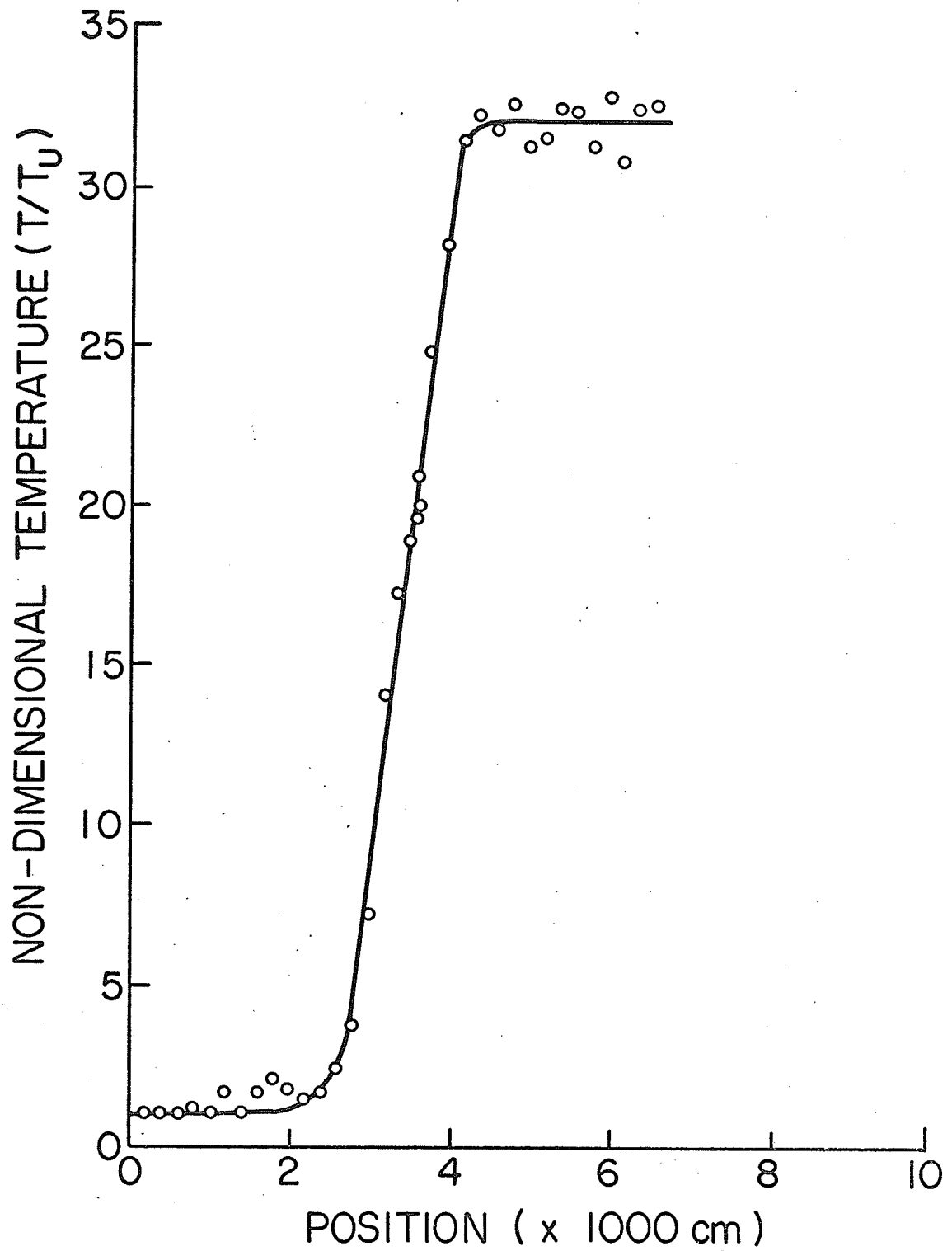


FIGURE 4 TEMPERATURE VARIATION WITH POSITION

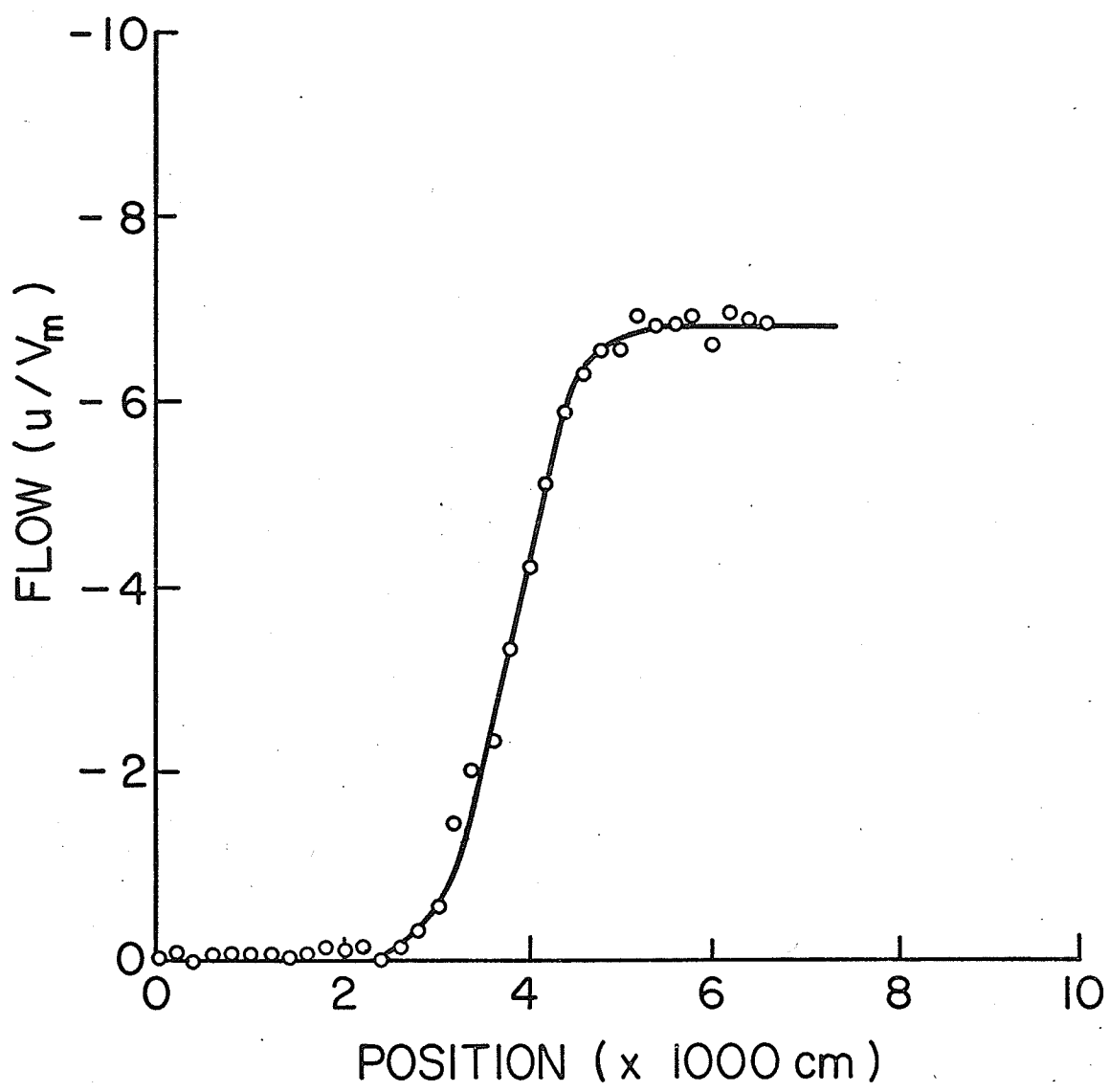


FIGURE 5 FLOW VARIATION WITH POSITION

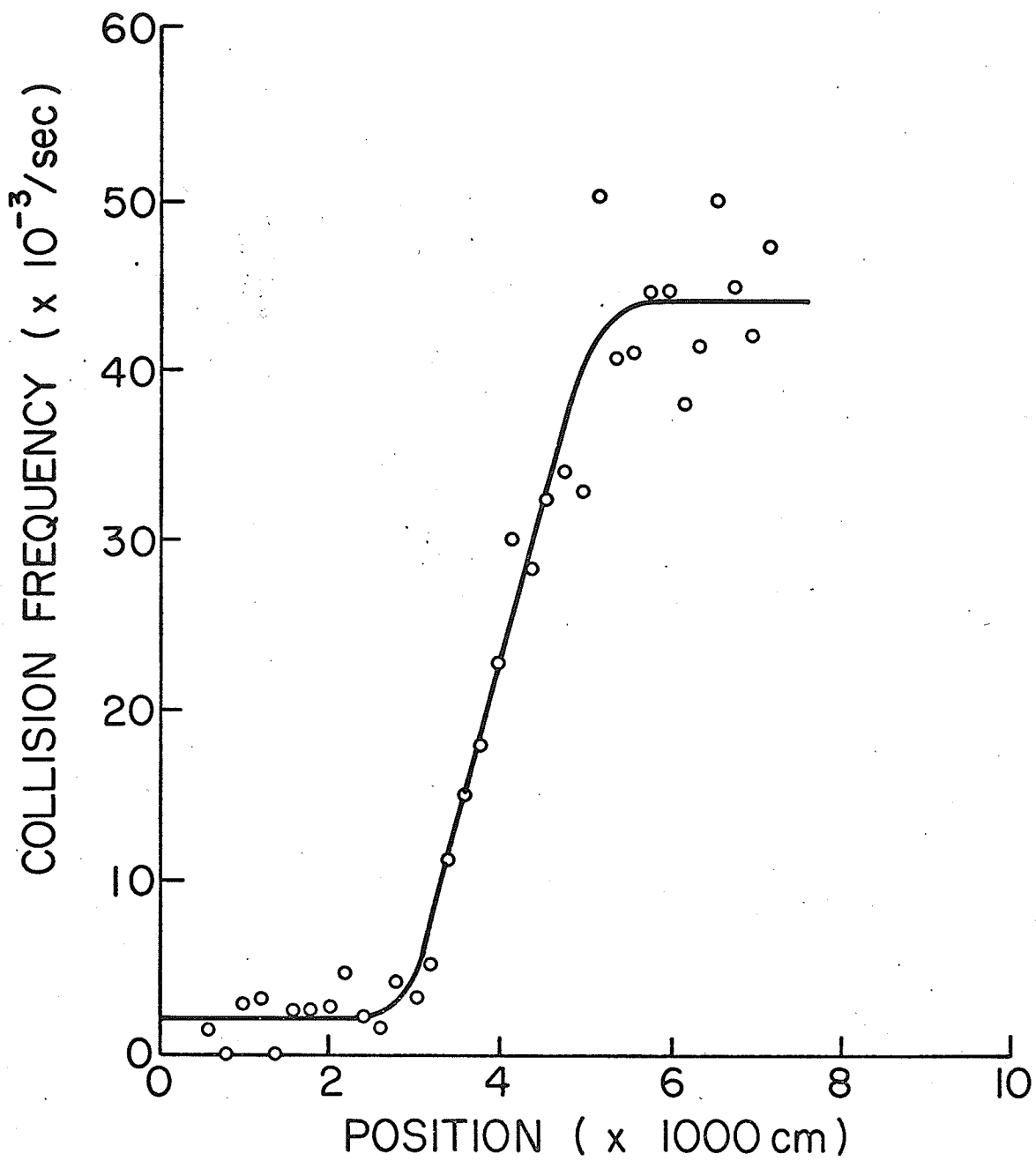


FIGURE 6 COLLISION FREQUENCY VARIATION WITH POSITION

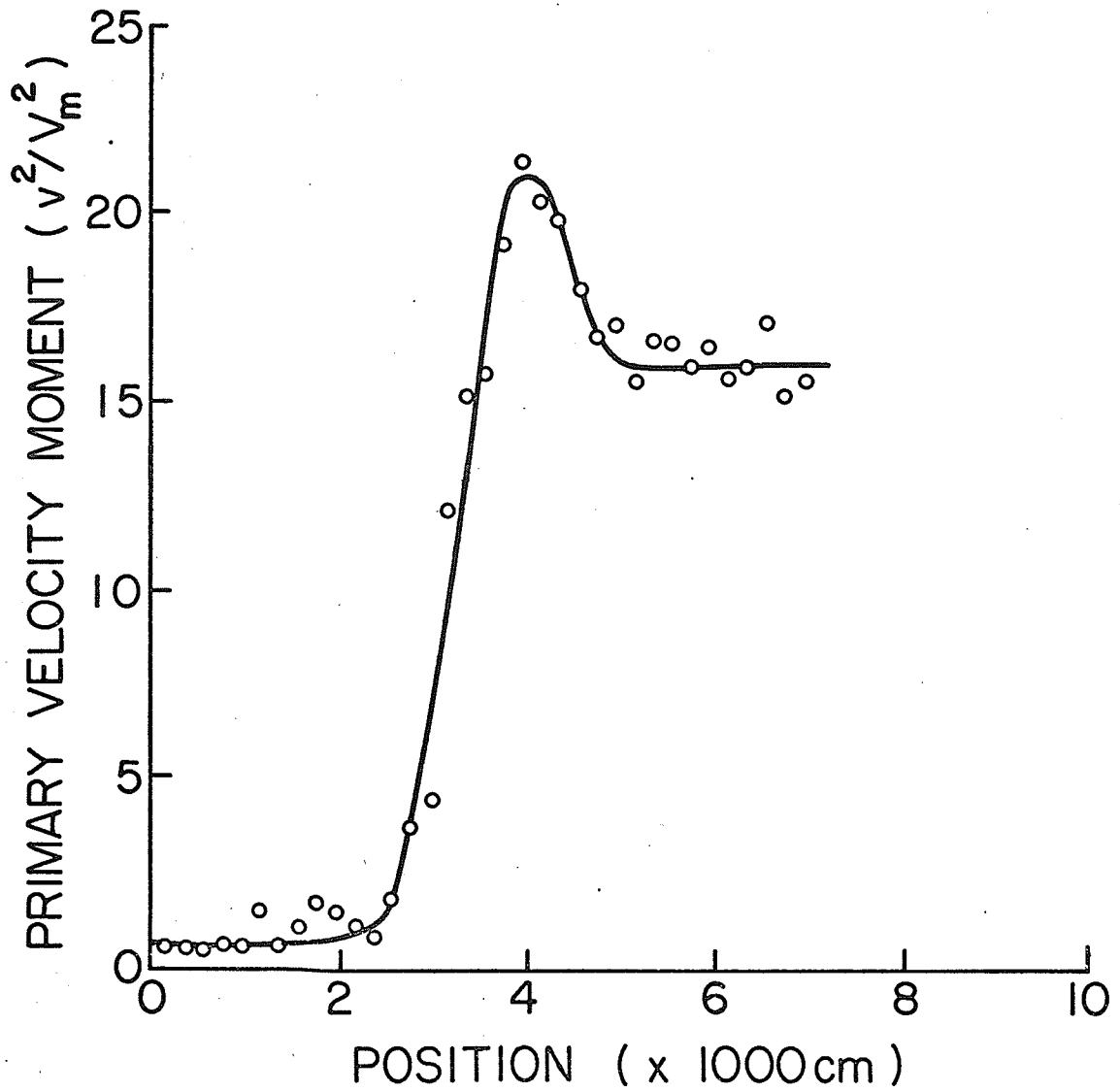


FIGURE 7 PRIMARY VELOCITY MOMENT VARIATION WITH POSITION

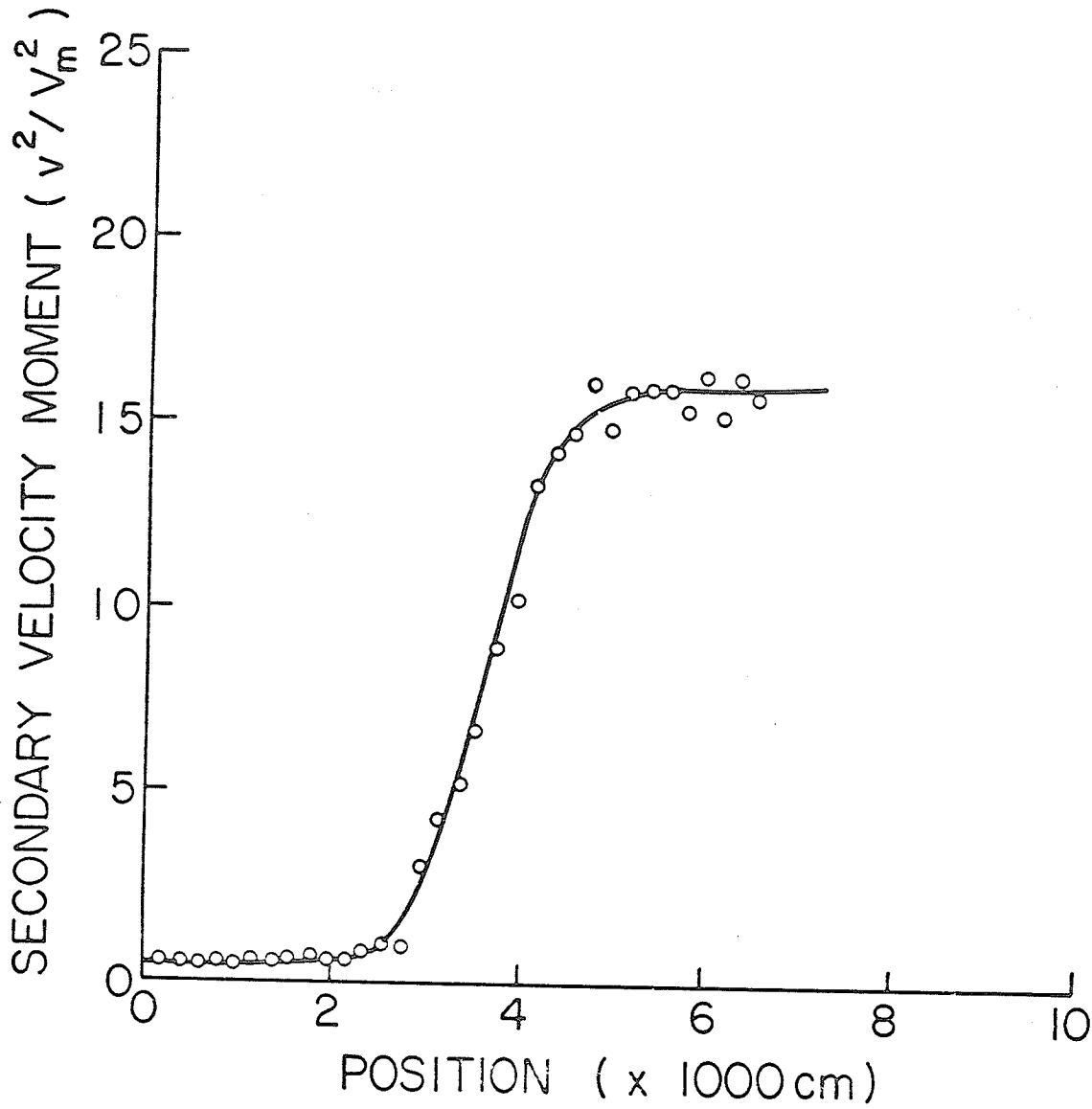


FIGURE 8 SECONDARY VELOCITY MOMENT VARIATION WITH POSITION

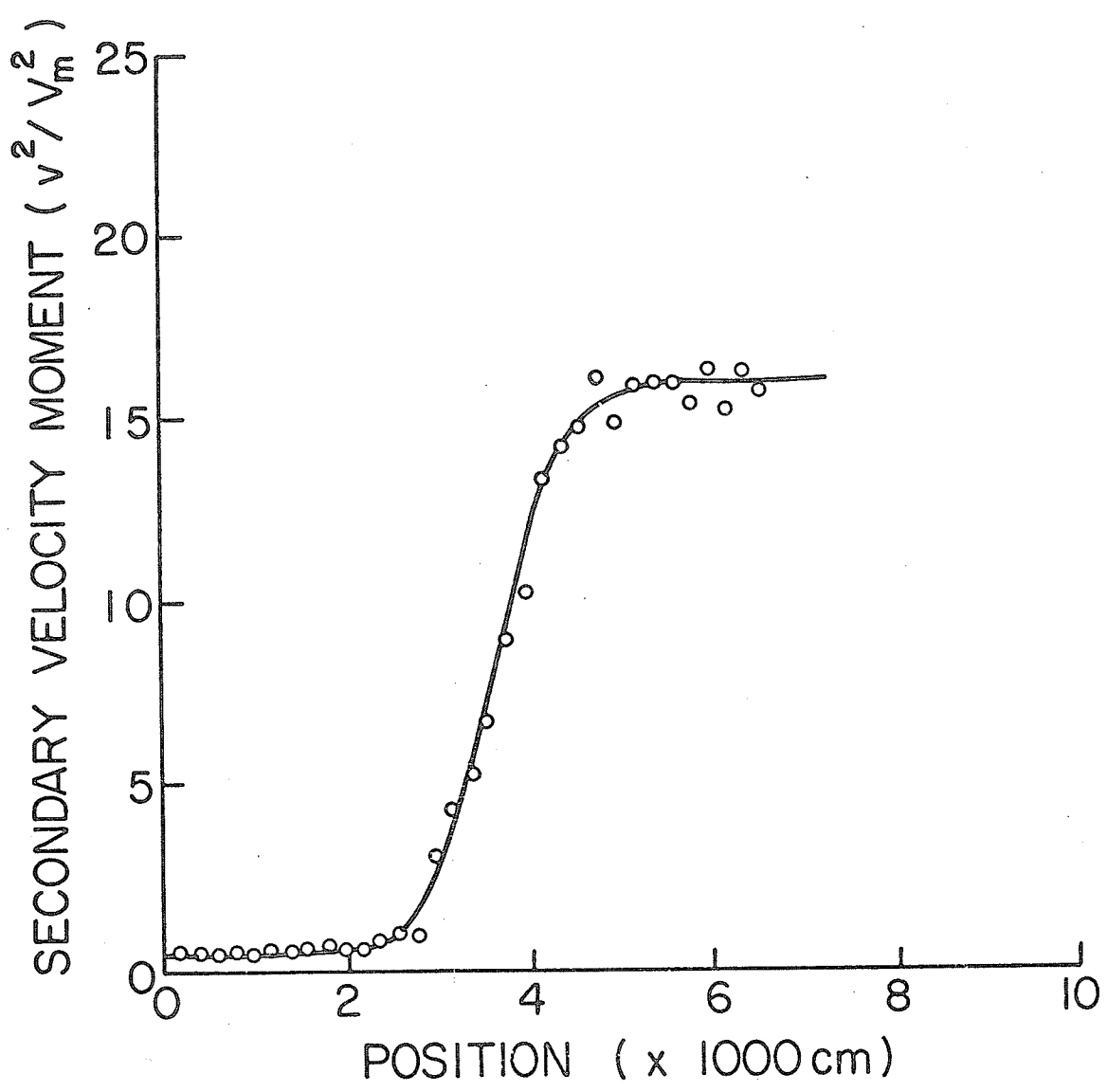


FIGURE 8 SECONDARY VELOCITY MOMENT VARIATIC WITH POSITION

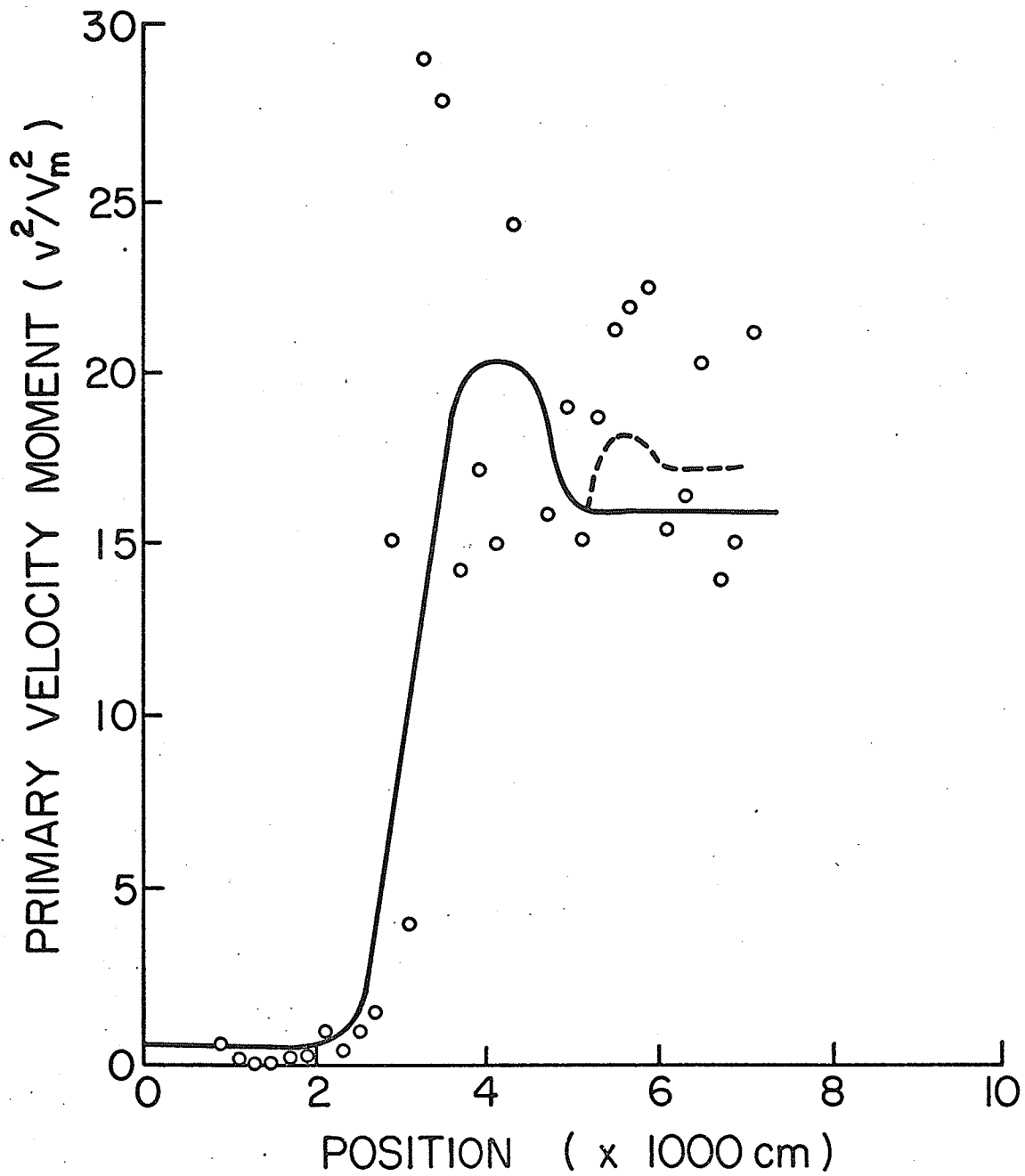


FIGURE 9 POST-COLLISIONAL PRIMARY VELOCITY MOMENT VARIATION WITH POSITION

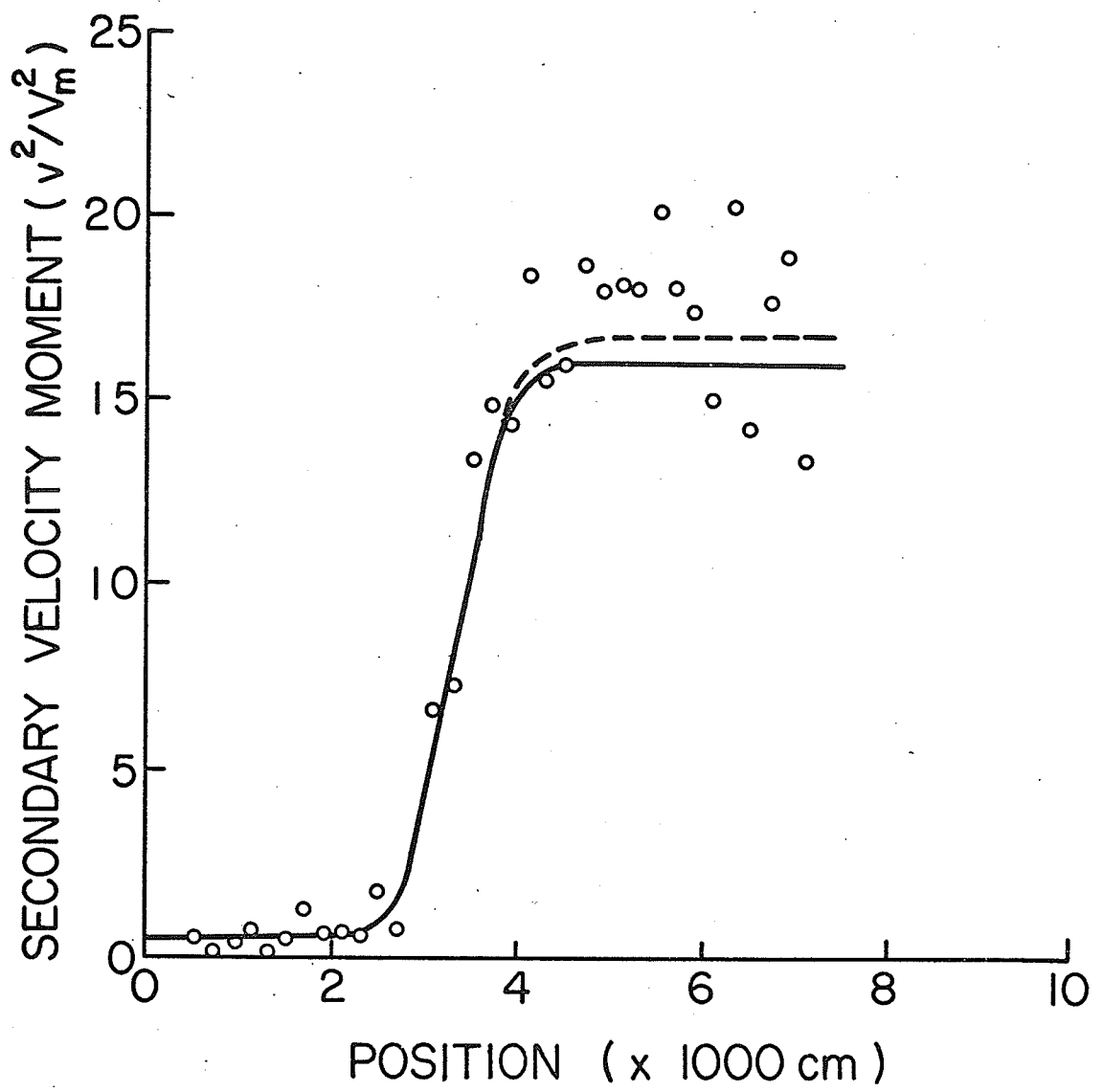


FIGURE 10 POST-COLLISIONAL SECONDARY VELOCITY MOMENT VARIATION WITH POSITION

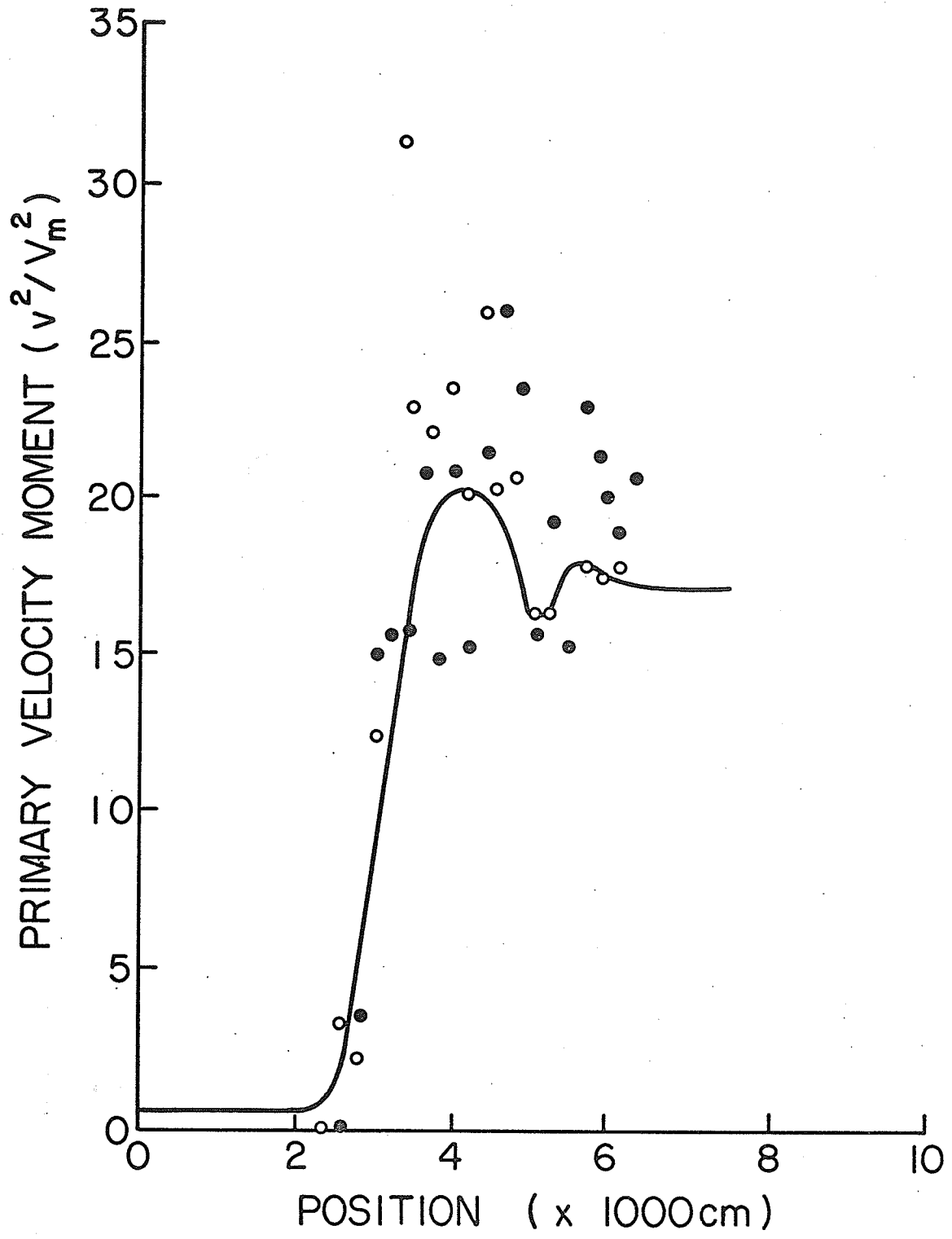


FIGURE II POST-COLLISIONAL PRIMARY VELOCITY MOMENT VARIATION AS PREDICTED BY TWO INDIVIDUAL DATA SETS

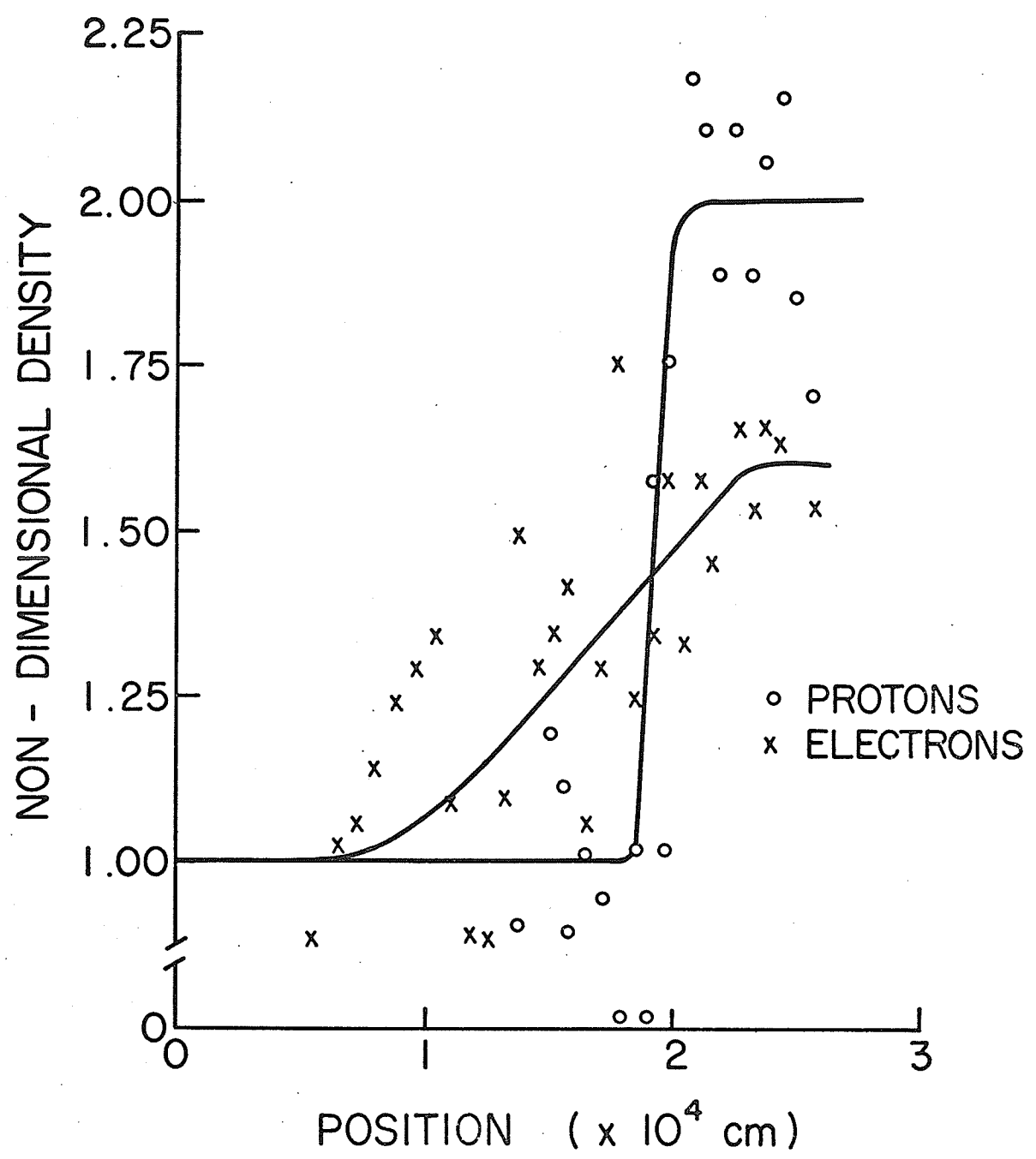


FIGURE 12 DENSITY PROFILES FOR ELECTRONS AND PROTONS

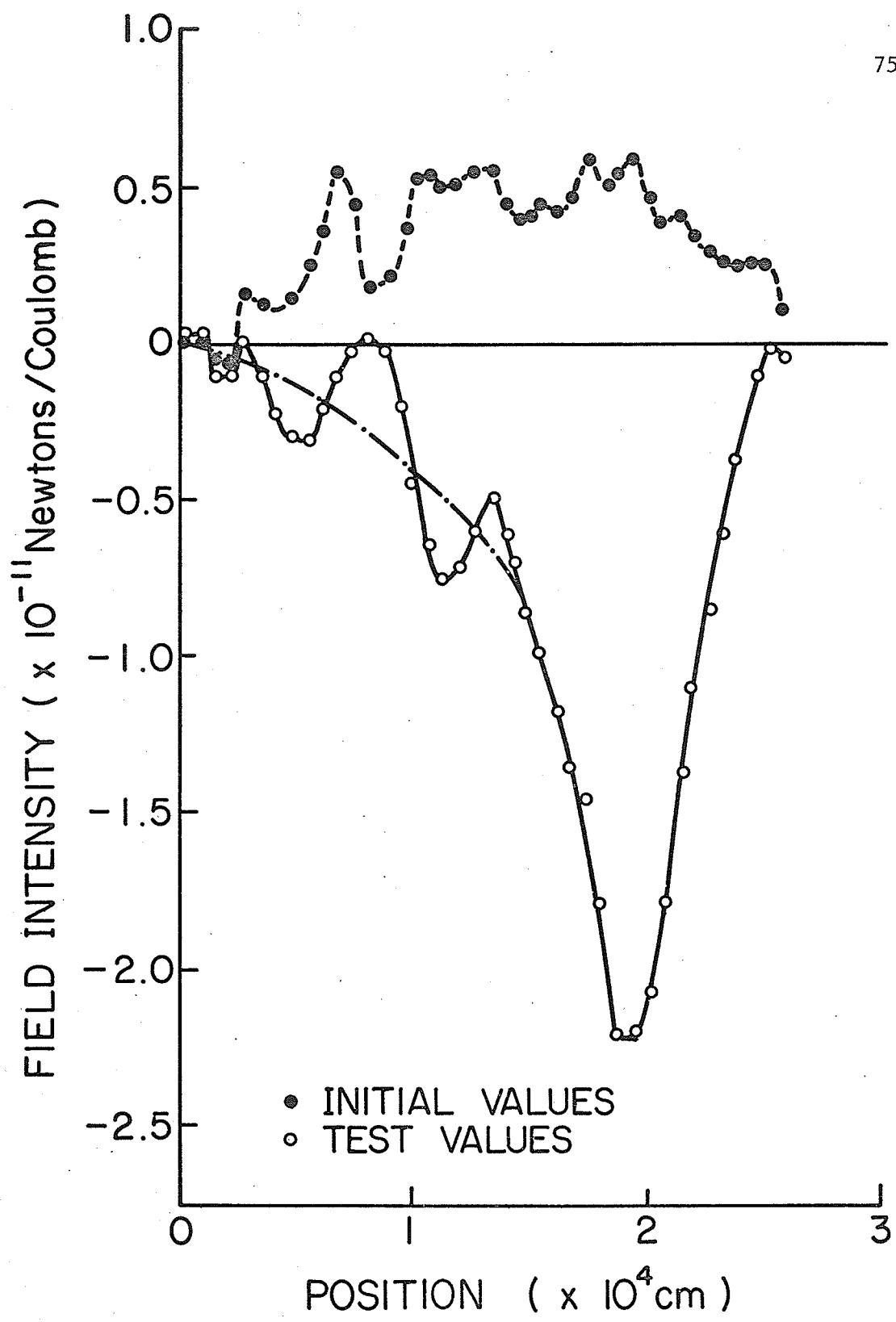


FIGURE 13 ELECTRIC FIELD VARIATION

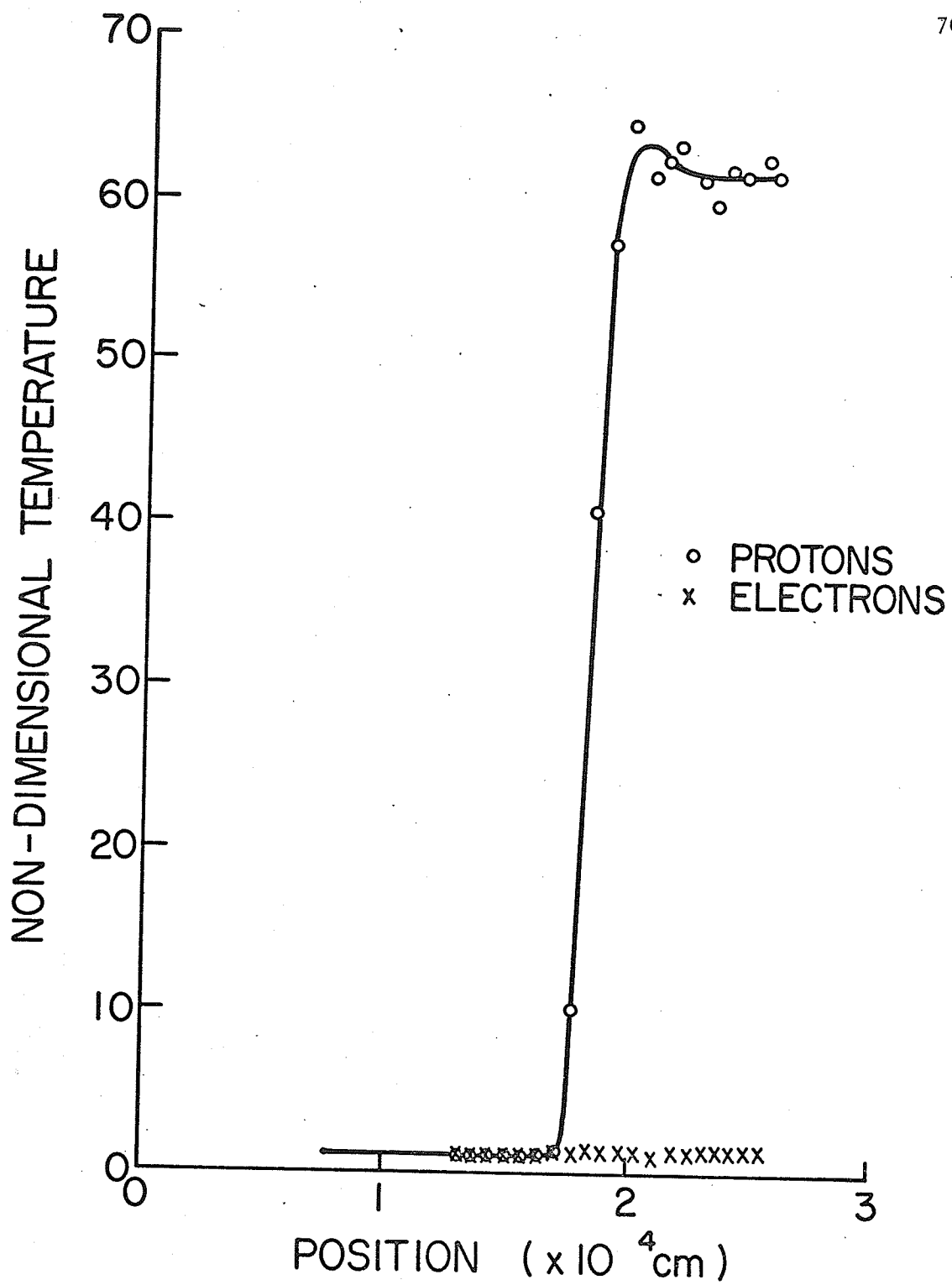


FIGURE 14 TEMPERATURE PROFILES FOR ELECTRONS AND PROTONS

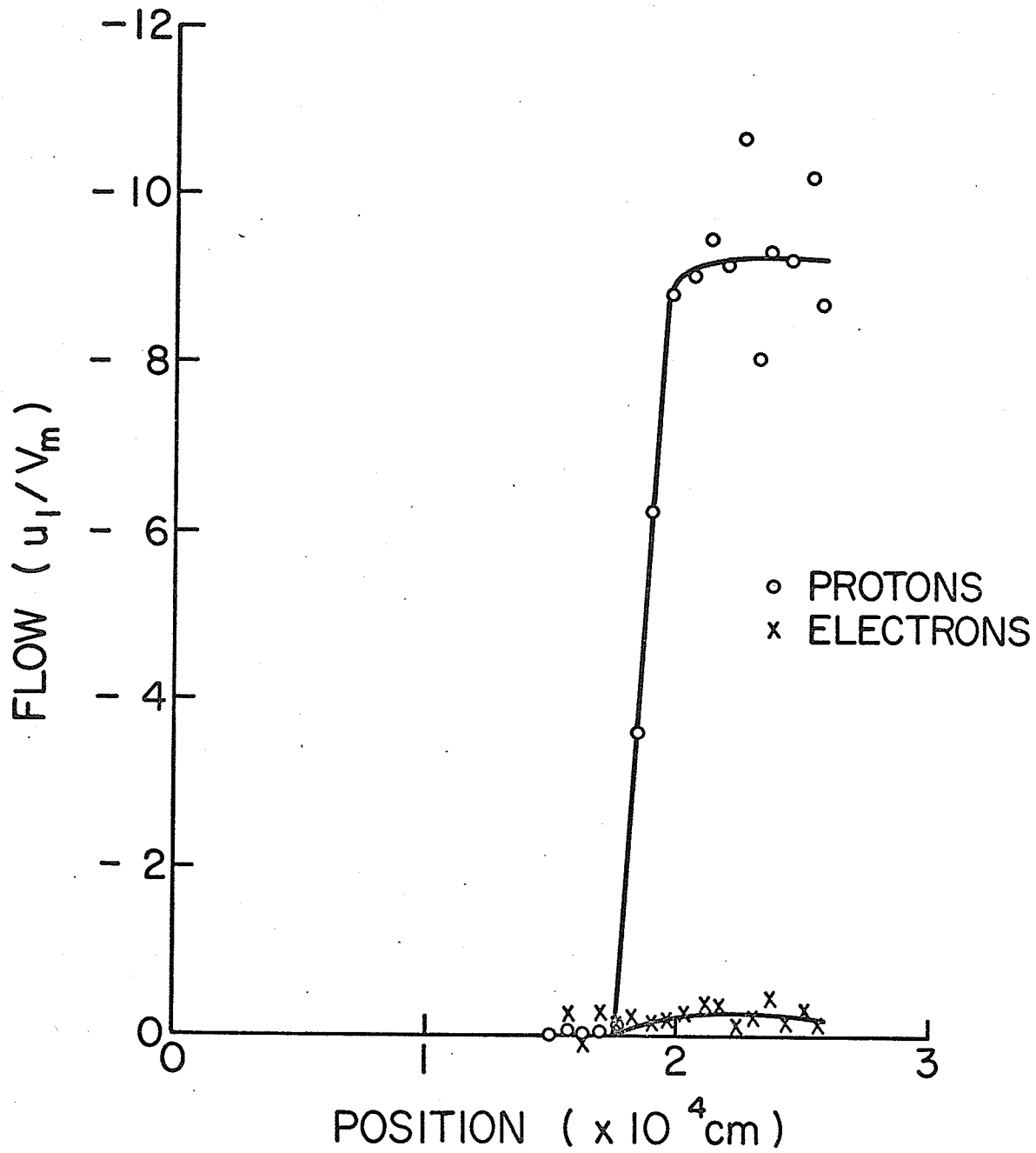


FIGURE 15 FLOW PROFILES FOR ELECTRONS AND PROTONS

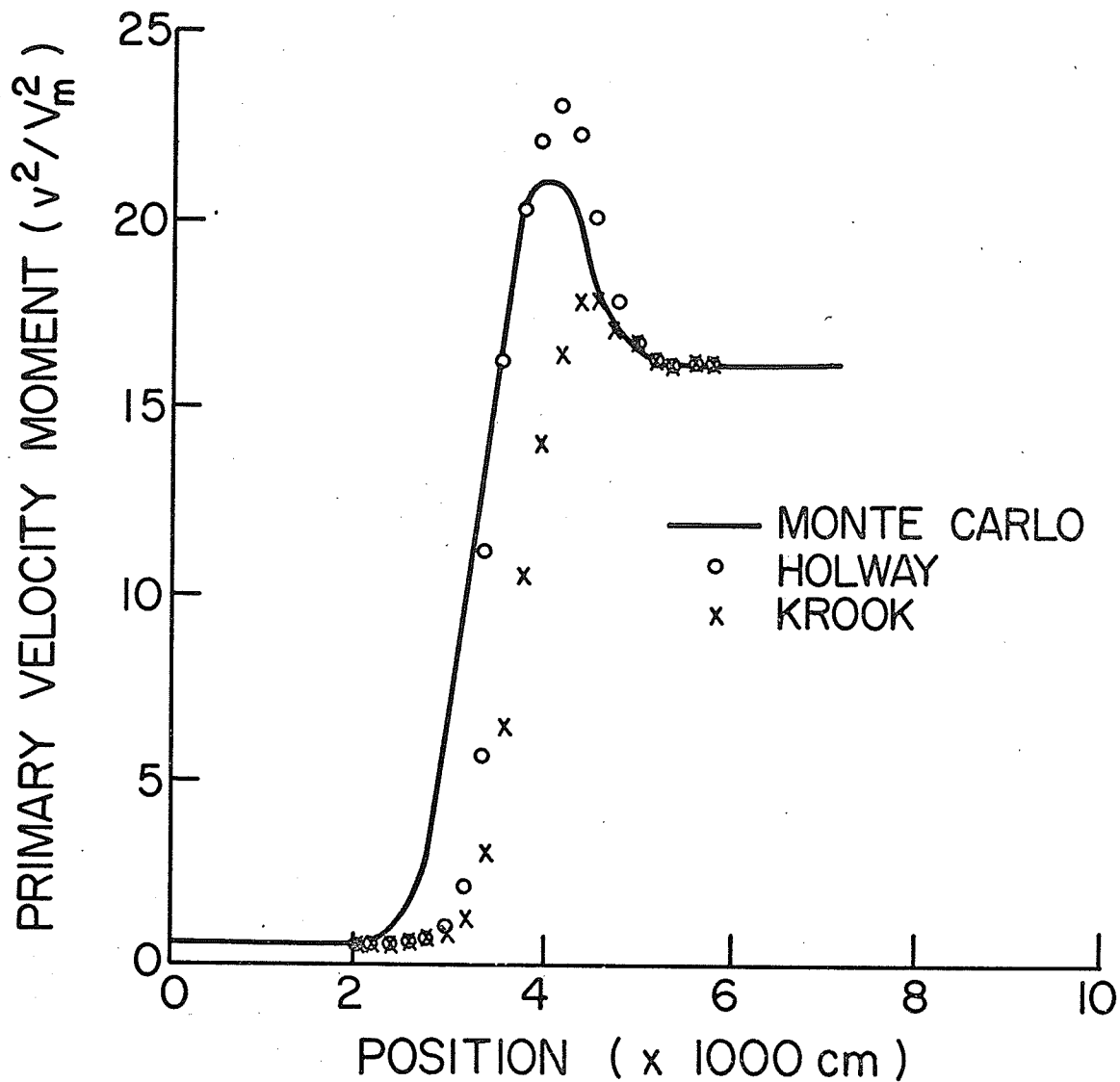


FIGURE 16 COMPARISON OF THE PRIMARY VELOCITY MOMENTS PREDICTED BY THE SIMULATION MODEL WITH THOSE PREDICTED BY THE INTEGRATION OF THE BOLTZMANN EQUATION USING HOLWAY'S FORMULATION AND KROOK'S FORMULATION

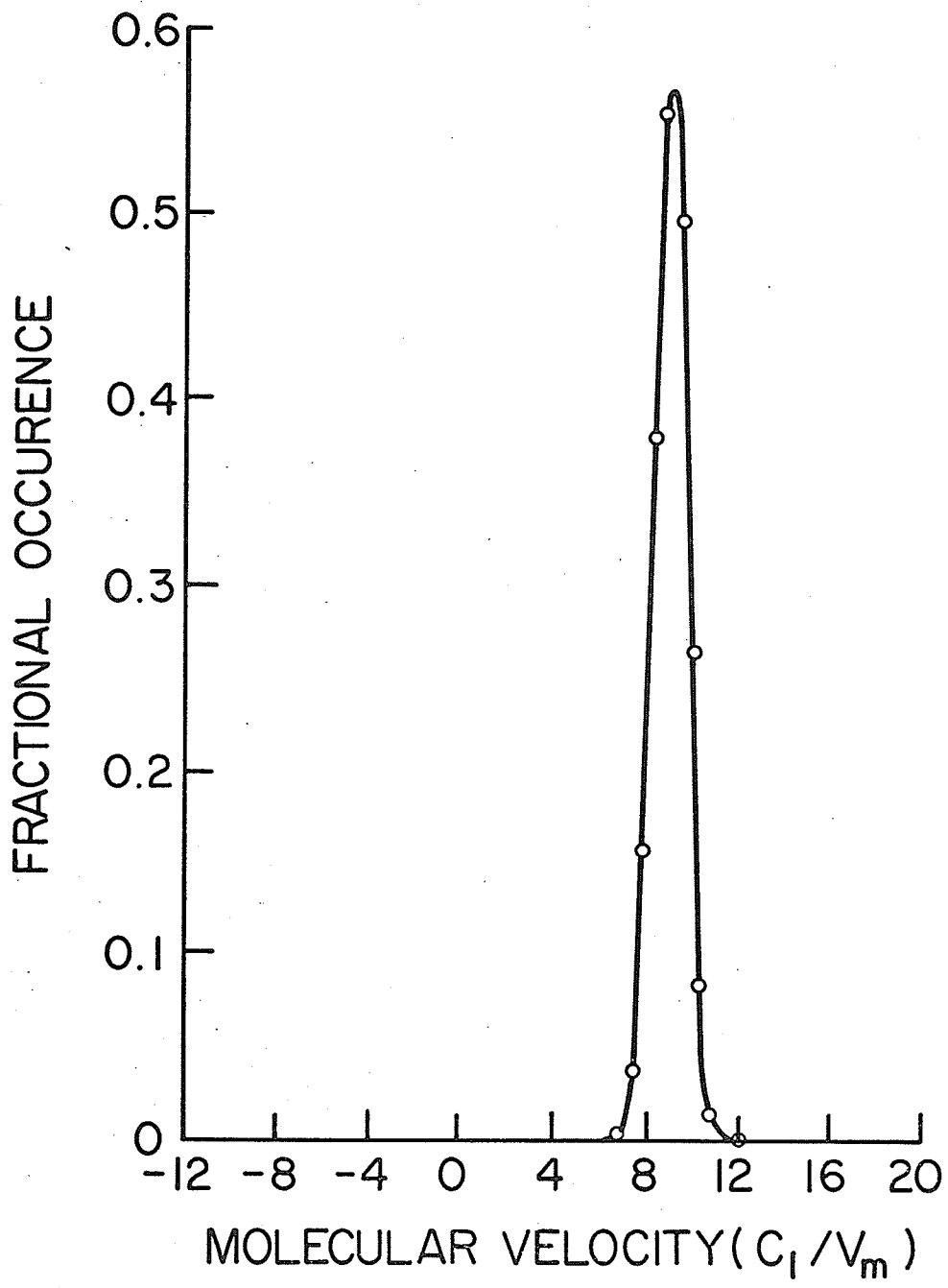


FIGURE 17 DISTRIBUTION FUNCTION, f_i , AT $r_i = 2.0 \times 10^{-3} \text{cm}$

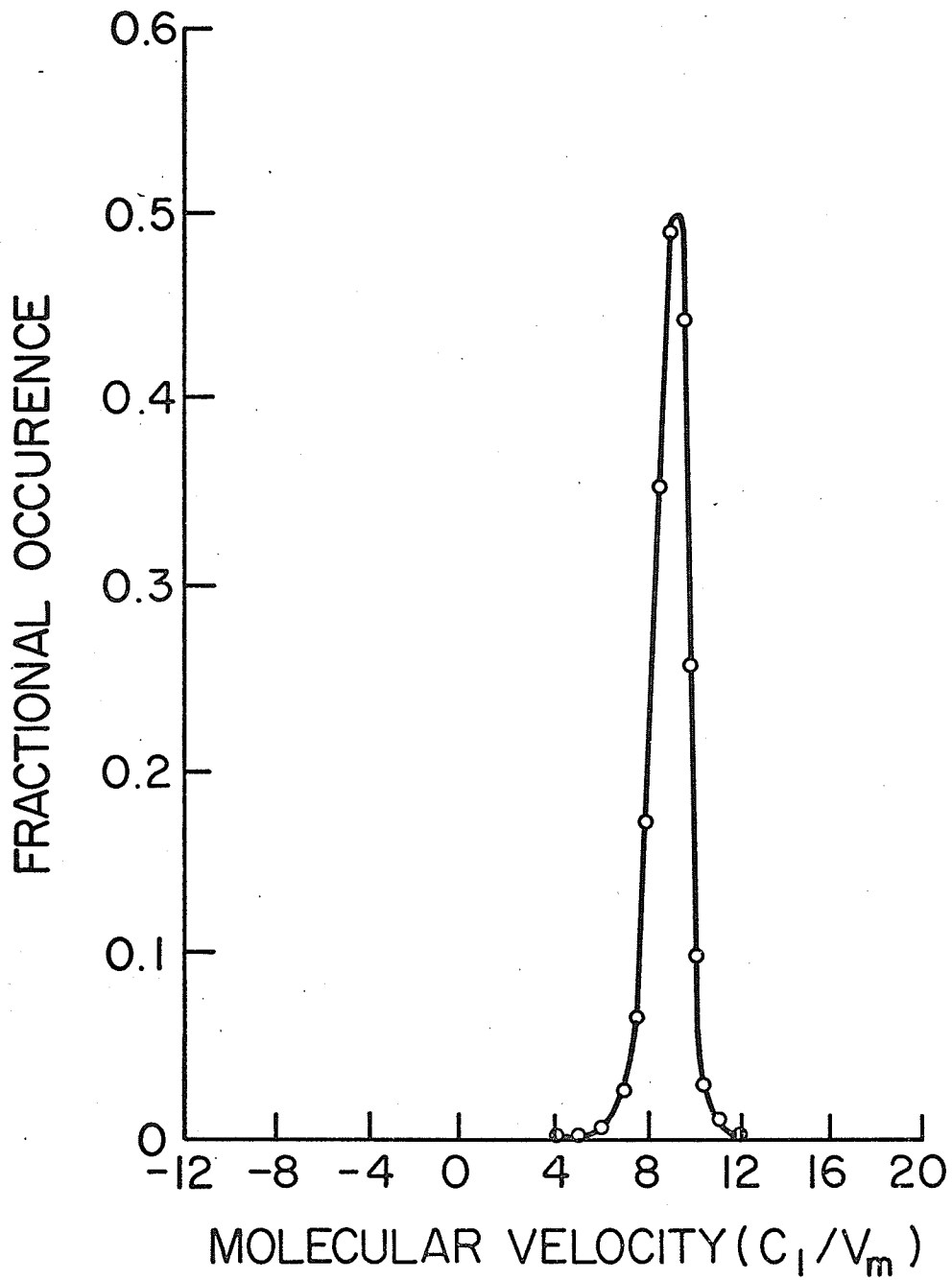


FIGURE 18 DISTRIBUTION FUNCTION, f_1 , AT
 $r_1 = 2.8 \times 10^{-3}$ cm

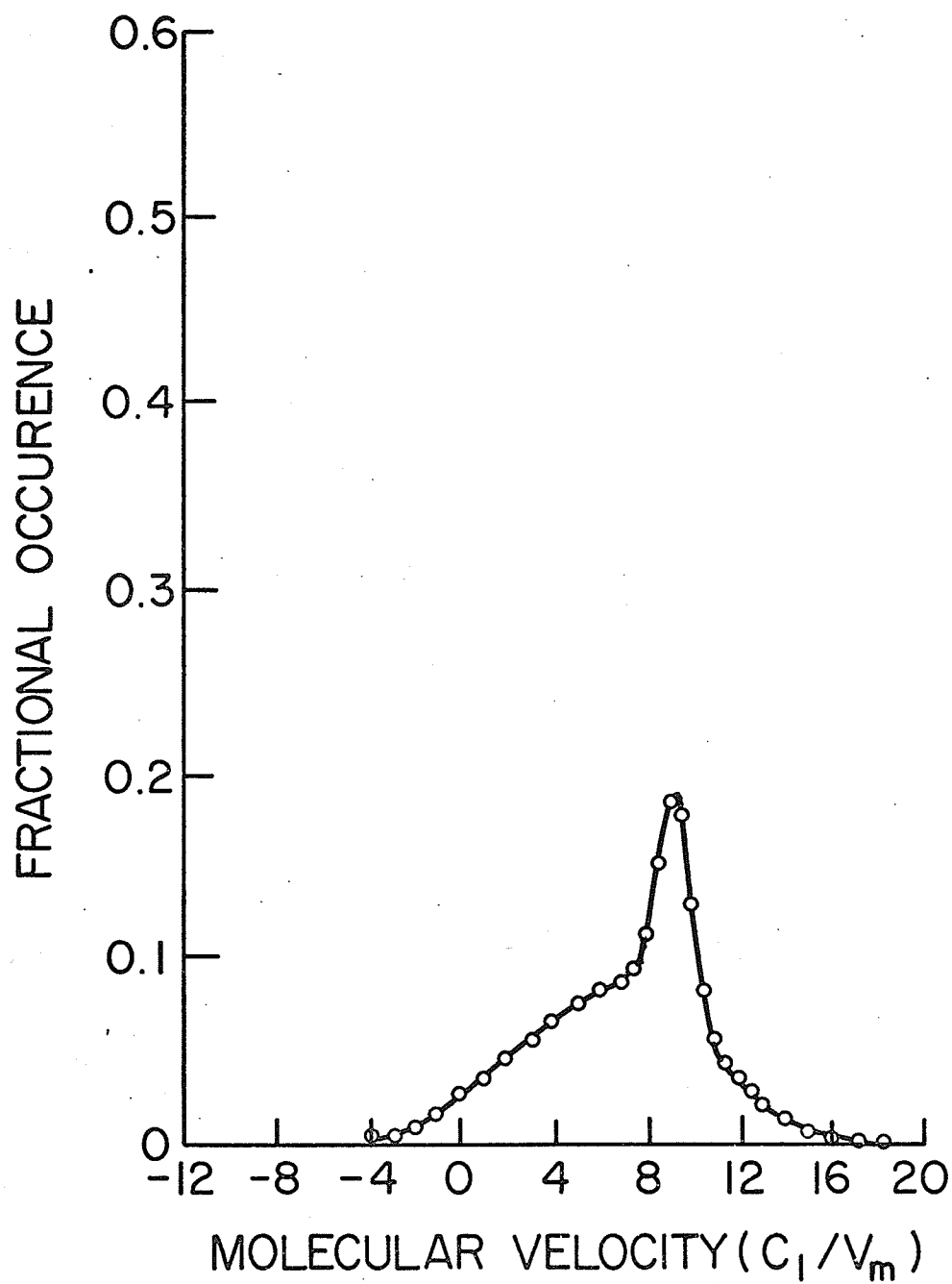


FIGURE 19 DISTRIBUTION FUNCTION, f_1 , AT
 $r_1 = 3.6 \times 10^{-3}$ cm

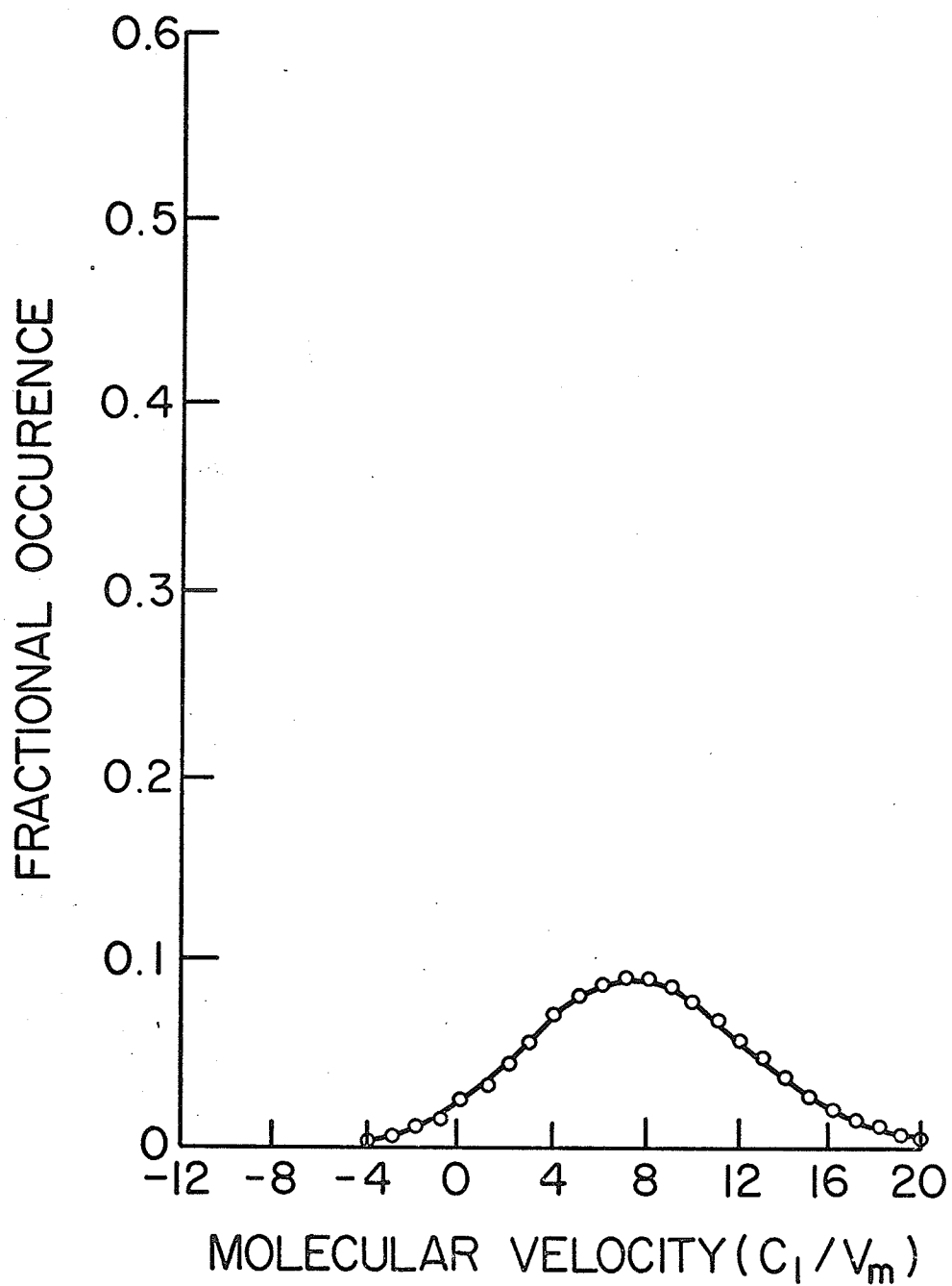


FIGURE 20 DISTRIBUTION FUNCTION, f_1 , AT
 $r_1 = 4.4 \times 10^{-3} \text{cm}$

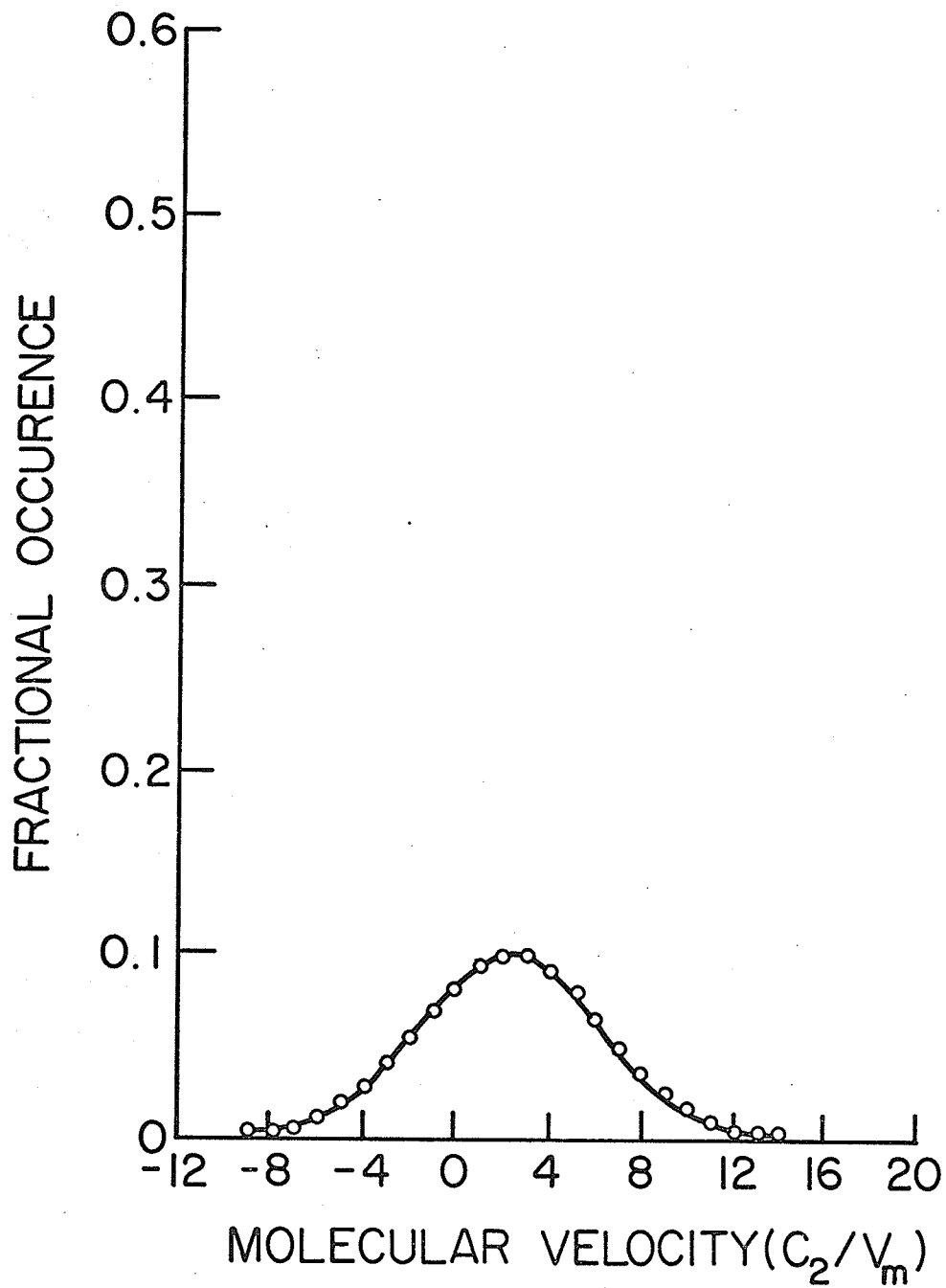


FIGURE 21 DISTRIBUTION FUNCTION, f_1 , AT
 $r_1 = 5.2 \times 10^{-3}$ cm (downstream position)

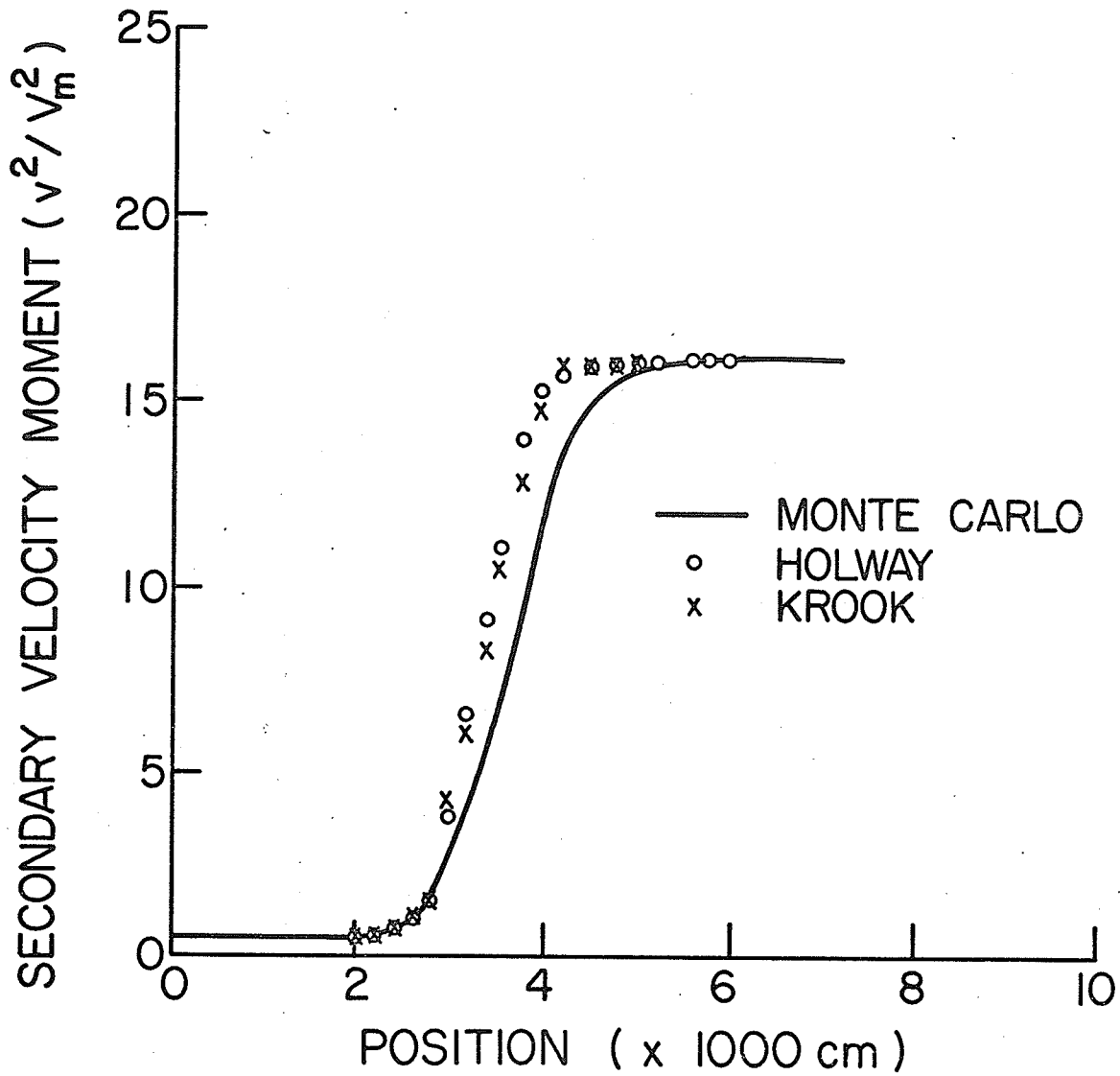


FIGURE 22 COMPARISON OF HOLWAY, KROOK AND MONTE CARLO PREDICTIONS FOR SECONDARY VELOCITY MOMENT

APPENDIX

APPENDIX I

Derivation of the Particles' Velocity Components After A Binary Collision

Consider two particles of mass m_1 and m_2 moving with velocities \underline{c}_1 and \underline{c}_2 respectively. The following parameters are defined

$$M_1 = \frac{m_1}{m_1 + m_2} \quad \text{A1-1a}$$

$$M_2 = \frac{m_2}{m_1 + m_2} \quad \text{A1-1b}$$

$$\underline{g}_{21} = \underline{c}_2 - \underline{c}_1 \quad \text{A1-2}$$

where \underline{g}_{21} is the relative velocity. Assuming these two particles collide, their velocities after collision are given in Chapman and Cowling¹¹ as

$$\underline{c}'_1 = \underline{c}_1 + 2 M_2 (\underline{g}_{21} \cdot \underline{k}) \underline{k} \quad \text{A1-3a}$$

$$\underline{c}'_2 = \underline{c}_2 - 2 M_1 (\underline{g}_{21} \cdot \underline{k}) \underline{k} \quad \text{A1-3b}$$

where \underline{k} is the collision vector and the only unknown.

Figure A1-1 is a diagram of a binary collision. \underline{k} is seen to be the bisecting vector of the two vectors \underline{g}_{21} and \underline{g}'_{21} . It is also observed that

$$\theta = \frac{\pi - \chi}{2} \quad \text{A1-4}$$

hence, \underline{k} is entirely specified by θ , therefore, χ , and an angle, η , which orientates the $\underline{g}_{21} - \underline{g}'_{21}$ plane in space. Henceforth, the unit vector \underline{g} will be defined as the unit vector in the direction of \underline{g}_{21} .

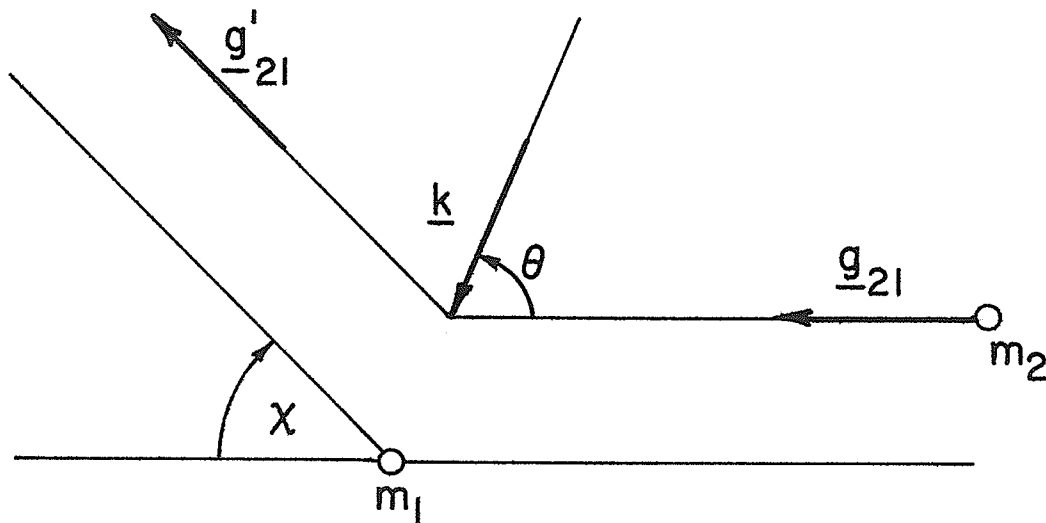


FIGURE A1-1: A BINARY COLLISION

If a plane, ξ , is constructed perpendicular to the \underline{g}_{21} vector, this plane intersects the x-y plane along a vector \underline{r} . (In the limit if ξ is identical to the x-y plane, \underline{r} will be defined as \underline{i} , the unit axis in the x direction.) The unit projection of the \underline{g} vector in the x-y plane is the vector

$$\underline{f} = \frac{g_1}{g_1 + g_2} \underline{i} + \frac{g_2}{g_1 + g_2} \underline{j} \quad \text{A1-5}$$

which makes an angle

$$\beta = \text{arc cos } (f_1) \quad \text{A1-6}$$

with the x-axis. Since \underline{r} and \underline{f} are at right angles to each other

\underline{r} makes an angle

$$\alpha = \beta - 90^\circ \quad \text{A1-7}$$

with the x-axis.

A right hand system of co-ordinates is defined by \underline{r} , \underline{g} and \underline{u} where

$$\underline{u} = \underline{r} \times \underline{g} \quad \text{A1-8a}$$

or

$$\underline{u} = r_2 g_3 \underline{i} - r_1 g_3 \underline{j} + (r_1 g_2 - r_2 g_1) \underline{n} \quad \text{A1-8b}$$

where \underline{i} , \underline{j} and \underline{n} are the original co-ordinate system. The ξ plane, in which both \underline{r} and \underline{u} lie, is then the plane in which η must lie to orientate the $\underline{g} - \underline{k}$ plane. Defining the vector \underline{q} to lie in both the ξ plane and the $\underline{g} - \underline{k}$ plane, \underline{q} is given by

$$\underline{q} = \cos \eta \underline{r} + \sin \eta \underline{u} \quad \text{A1-9}$$

and \underline{k} is

$$\underline{k} = \cos \theta \underline{g} + \sin \theta \underline{q} \quad \text{A1-10}$$

The expanded components of \underline{k} are

$$k_1 = \cos \theta g_1 + \sin \theta \cos \eta \cos \alpha + \sin \theta \sin \eta \sin \alpha g_3 \quad \text{A1-11a}$$

$$k_2 = \cos \theta g_2 + \sin \theta \cos \eta \sin \alpha - \sin \theta \sin \eta \cos \alpha g_3 \quad \text{A1-11b}$$

$$k_3 = \cos \theta g_3 + \sin \theta \sin \eta (\cos \alpha g_2 - \sin \alpha g_1) \quad \text{A1-11c}$$

Since θ has been shown to be a function of χ , the components of velocity after collision are obtainable from initial conditions and a knowledge of χ and η .

APPENDIX II

A Derivation of the One-Dimensional Statistically Modeled Boltzmann Equation

The general form of Boltzmann's equation is

$$\frac{\partial f}{\partial t} + \underline{c} \cdot \frac{\partial f}{\partial \underline{r}} + \underline{a} \cdot \frac{\partial f}{\partial \underline{c}} = \left(\frac{\partial f}{\partial t} \right)_{\text{col}} \quad \text{A2-1}$$

where f is the normalized distribution function, t is the time, \underline{c} is the molecular velocity, \underline{r} is the position and \underline{a} is the acceleration due to external fields. The BGK model of the collision term (right hand side of equation A2-1) is

$$\left(\frac{\partial f}{\partial t} \right)_{\text{col}} = \nu (\psi - f) \quad \text{A2-2}$$

where ν is the collision frequency and ψ is the velocity distribution of molecules emerging from a collision.

Expanding equation A2-1 and substituting equation A2-2, it is seen that

$$\begin{aligned} \frac{\partial f}{\partial t} + c_1 \frac{\partial f}{\partial r_1} + c_2 \frac{\partial f}{\partial r_2} + c_3 \frac{\partial f}{\partial r_3} + a_1 \frac{\partial f}{\partial c_1} + a_2 \frac{\partial f}{\partial c_2} + a_3 \frac{\partial f}{\partial c_3} \\ = \nu (\psi - f) \end{aligned} \quad \text{A2-3}$$

Assuming a steady state shock wave in the r_1 direction with no external field

$$\frac{\partial f}{\partial t} = 0 \quad \text{A2-4a}$$

$$\frac{\partial f}{\partial r_2} = \frac{\partial f}{\partial r_3} = 0$$

A2-4b

$$a_1 = a_2 = a_3 = 0$$

A2-4c

and equation A2-3 reduces to

$$c_1 \frac{\partial f}{\partial r_1} = v(\psi - f)$$

A2-5

By definition

$$f = f_1 f_2 f_3$$

A2-6a

$$\psi = \psi_1 \psi_2 \psi_3$$

A2-6b

where the subscripts denote the component equations. It follows that

$$\frac{\partial f}{\partial r_1} = f_1 f_2 \frac{\partial f_3}{\partial r_1} + f_2 f_3 \frac{\partial f_2}{\partial r_1} + f_2 f_3 \frac{\partial f_1}{\partial r_1}$$

A2-7

Integrating equation A2-5 over all c_2 and c_3 and noting that

$$\int_{-\infty}^{\infty} f_i dc_i = 1$$

A2-8a

$$\int_{-\infty}^{\infty} \frac{\partial f_i}{\partial r_2} dc_i = \frac{\partial}{\partial r_1} \int_{-\infty}^{\infty} f_i dc_i = 0$$

A2-8b

(where i is either 2 or 3) it is found that

$$c_1 \frac{\partial f_1}{\partial r_1} = v(\psi_1 - f_1)$$

A2-9

Similarly, an integration over all c_1 and c_3 yields

$$f_2 = \psi_2$$

A2-10

and over all c_1 and c_3 the result is

$$f_3 = \psi_3$$

A2-11

APPENDIX III

A Derivation of the One-Dimensional Velocity Distribution Function of Molecules Coming Out of Collision

Holway¹⁶ gives the velocity distribution function of molecules emerging from collision, ψ , as

$$\psi = (2\pi)^{-\frac{3}{2}} |\underline{\lambda}|^{-\frac{1}{2}} \exp -\frac{1}{2} \left(\epsilon_{ij} (c_i - u_i) (c_j - u_j) \right) \quad \text{A3-1}$$

where $\underline{\lambda}$ is the velocity moment matrix of such molecules, $\underline{\epsilon}$ is the tensor inverse of $\underline{\lambda}$, \underline{c} is the molecular velocity and \underline{u} is the flow. Defining the peculiar velocity by \underline{v} where

$$\underline{v} = \underline{c} - \underline{u}$$

equation A3-1 may be expanded as

$$\psi = (2\pi)^{-\frac{3}{2}} |\underline{\lambda}|^{-\frac{1}{2}} \exp -\frac{1}{2} \left(\epsilon_{11} v_1^2 + \epsilon_{22} v_2^2 + \epsilon_{33} v_3^2 + 2 \epsilon_{12} v_1 v_2 + 2 \epsilon_{13} v_1 v_3 + 2 \epsilon_{23} v_2 v_3 \right) \quad \text{A3-2}$$

(Note: Since $\underline{\lambda}$ is symmetric, $\underline{\epsilon}$ is also symmetric and $\epsilon_{21} = \epsilon_{12}$, $\epsilon_{31} = \epsilon_{13}$ and $\epsilon_{32} = \epsilon_{23}$).

the one-dimensional form, ψ_1 is obtained by integrating over all v_2 . It follows that

$$\psi_1 = (2\pi)^{-\frac{3}{2}} |\underline{\lambda}|^{-\frac{1}{2}} \exp -\frac{1}{2} \epsilon_{11} v_1^2 \int_{-\infty}^{\infty} \exp -\frac{1}{2} (\epsilon_{33} v_3^2 + 2 \epsilon_{13} v_1 v_3)$$

(over)

$$\left(\int_{-\infty}^{\infty} \exp - \frac{1}{2} \left(\epsilon_{22} v_2^2 + 2 \left[\epsilon_{12} v_1 + \epsilon_{13} v_3 \right] v_2 \right) dv_2 \right) dv_3 \quad \text{A3-3}$$

By completing the square of the inner integral this integral reduces to

$$\exp \frac{(\epsilon_{12} v_1 + \epsilon_{23} v_3)^2}{2 \epsilon_{22}} \int_{-\infty}^{\infty} \exp - \frac{1}{2} \left(\epsilon_{22} v_2 + \frac{\epsilon_{12} v_1 + \epsilon_{23} v_3}{\epsilon_{22}} \right)^2 dv_2$$

which is of the form

$$\frac{1}{\epsilon_{22}} \int_{-\infty}^{\infty} \exp - \frac{1}{2} z^2 dz$$

and has the solution

$$\left(\frac{2\pi}{\epsilon_{22}} \right)^{1/2} \exp \frac{(\epsilon_{12} v_1 + \epsilon_{23} v_3)^2}{2 \epsilon_{22}}$$

Equation A3-3 now takes the form

$$\psi_1 = \frac{1}{2\pi \epsilon_{22} |\underline{\lambda}|^{1/2}} \exp - \frac{1}{2} \left(\epsilon_{11} v_1^2 - \frac{\epsilon_{12}^2 v_1^2}{\epsilon_{22}} \right) \int_{-\infty}^{\infty} \exp - \frac{1}{2} \left(\left(\epsilon_{33} - \frac{\epsilon_{23}^2}{\epsilon_{22}} \right) v_3^2 + 2 \left(\epsilon_{13} v_1 - \frac{\epsilon_{12} \epsilon_{23}}{\epsilon_{22}} v_1 \right) v_3 \right) dv_3 \quad \text{A3-4}$$

Once more employing a completing the square technique the resultant

equation is

$$\psi_1 = \left[2\pi \left(\epsilon_{22} \epsilon_{33} - \epsilon_{23}^2 \right) \left| \underline{\lambda} \right| \right]^{-1/2}$$

$$\exp - \frac{v_1^2}{2} \left[\epsilon_{11} - \frac{\epsilon_{12}^2 \epsilon_{33} + \epsilon_{13}^2 \epsilon_{22} - 2 \epsilon_{12} \epsilon_{13} \epsilon_{23}}{\epsilon_{22} \epsilon_{33} - \epsilon_{23}^2} \right] \quad \text{A3-5}$$

By analogous techniques the second and third component equations,

ψ_2 and ψ_3 , are

$$\psi_2 = \left[2\pi \left(\epsilon_{11} \epsilon_{33} - \epsilon_{13}^2 \right) \left| \underline{\lambda} \right| \right]^{-1/2}$$

$$\exp - \frac{v_2^2}{2} \left[\epsilon_{22} - \frac{\epsilon_{12}^2 \epsilon_{11} + \epsilon_{23}^2 \epsilon_{33} - 2 \epsilon_{12} \epsilon_{13} \epsilon_{23}}{\epsilon_{11} \epsilon_{33} - \epsilon_{13}^2} \right] \quad \text{A3-6}$$

$$\psi_3 = \left[2\pi \left(\epsilon_{11} \epsilon_{22} - \epsilon_{12}^2 \right) \left| \underline{\lambda} \right| \right]^{-1/2}$$

$$\exp - \frac{v_3^2}{2} \left[\epsilon_{33} - \frac{\epsilon_{13}^2 \epsilon_{11} + \epsilon_{23}^2 \epsilon_{22} - 2 \epsilon_{12} \epsilon_{13} \epsilon_{23}}{\epsilon_{11} \epsilon_{22} - \epsilon_{12}^2} \right] \quad \text{A3-7}$$